Design scenarios of outdoor arrayed cylindrical photobioreactors for microalgae cultivation considering solar radiation and temperature

Jianke Huang [a], Ben Hankamer [b], Jennifer Yarnold [c *]

[a] State Key Laboratory of Bioreactor Engineering, East China University of Science and Technology, Shanghai, PR China

[b] Institute for Molecular Bioscience, The University of Queensland, Queensland, Australia

[b] Centre for Policy Futures, The University of Queensland, Queensland, Australia

Corresponding authors: Jennifer Yarnold and Ben Hankamer

Email: j.yarnold@uq.edu.au and b.hankamer@imb.uq.edu.au

https://doi.org/10.1016/j.algal.2019.101515

Abstract

Advancing microalgae biotechnologies requires the design of high efficiency, large scale outdoor photobioreactor systems. Here we present a predictive biomass productivity model to define system design parameters yielding high biomass productivities for a facility encompassing arrays of cylindrical photobioreactors (PBRs) in a sub-tropical location (Brisbane, Australia). The model analyses the temperature and the light distributed through the culture medium as a function of PBR height, diameter, spacing distance between reactors, biomass concentration and cultivation regime (continuous vs. batch; fixed vs. capped temperature control). Temporal changes in light and temperature were used to predict volumetric and areal productivities (P_{vol} and P_{areal} respectively) for three *Chlorella* strains (*C. vulgaris, C. sp*. 11_H5 and *C. pyrenoidosa*). A simple empirical relationship was derived to rapidly predict P_{vol} in PBR arrays based on the ratio of spacing distance and reactor height (*L/H*) if the P_{vol} of a single, unshaded PBR was known. For *C. vulgaris* under a continuous operation and variable temperature (within its maximum growth threshold), the highest P_{vol} in the range analysed was obtained at the smallest diameter (0.1 m), highest biomass concentration (1.5 g L^{-1}) and largest *L/H*, (P_{vol} ~0.3 g L^{-1} d^{-1}). In contrast, the highest P_{areal} (~50 t ha^{-1} yr^{-1}) was found at higher diameters (0.15 and 0.3 m), a lower biomass concentration (0.3 g L^{-1}) and low *L/H* (0.2-0.4); this was attributed to a higher overall culture volume per PBR and per area. Our predictions, based on light and temperature effects on productivity, suggest that attaining a high P_{vol} could reduce costs, energy and materials associated with water usage, harvest loads and PBRs; whereas attaining a P_{areal} toward its maxima could reduce costs associated with land. The model supports effective PBR array design and process optimisation to help minimise production cost.

Keywords

Cylindrical photobioreactor; microalgae; predictive model; biomass; temperature; light

Nomenclature

Cp_w	Specific heat capacity of culture broth (J kg^{-1} K^{-1})	P_{vol}	Annual average volumetric productivity(g dry weight L^{-1} d^{-1})
C_x	Dry weight biomass concentration (g L^{-1})	$P_{vol\text{-}light}$	Annual average volumetric productivity during the light period of day(g dry weight L^{-1} d^{-1})
$C_{x\ initial}$	Initial dry weight biomass concentration for batch culture	P_{vol_s}	Annual average volumetric productivity of a single, isolated PBR during the light period of day(g dry weight L^{-1} d^{-1})
C_{x_end}	Dry weight biomass concentration of batch end (g L^{-1})	P(i)	Dry weight biomass productivity of i batch cultivation
D	Reactor diameter (m)	Q	Radiation or heat flow for temperature calculation (W)
D_{EW}	Distance between neighboring reactor in east-west direction(center to center)(m)	R	Reactor radius(m)
Di	Dilution rate (h^{-1})	r	Polar radius of any point inside the reactor in polar coordinate system(m)
D_{NS}	Distance between neighboring reactor in south-north direction(center to center)(m)	r_d	Maintenance coefficient of microalgae(h^{-1})
H	Total height of reactor, including reactor height and base height(m)	T_{app}	Strain's appropriate temperature(℃)
H_{base}	Base height(m)	T_{min}	Temperature below which the growth is assumed to be zero(℃)
H_d	Daily radiation (W m^{-2})	T_{max}	Temperature above which there is no growth(℃)
H_O	Daily extraterrestrial radiation (W m^{-2})	T_{opt}	Strain's optimal temperature(℃)
H_{PBR}	Reactor height(m)	T_r	reactor liquid temperature(K)
H_{shaded}	Height reactor shaded(m)	u	Sky view angle(°)
h	Reactor height measured from the bottom(m)	u'	Sky view angle for ground reflection
h'	Reactor height measured from the top of column(m)		
i	Batch number	V_r	Volume of culture broth in PBR for temperature calculation(m^3)
I_0	Light intensity (μmol m^{-2} s^{-1})		
I_{diff}	Diffuse light intensity(μmol m^{-2} s^{-1})	α	Initial slope of the light response curve for *C. Pyrenoidosa*
I_{dire}	Direct light intensity(μmol m^{-2} s^{-1})	β	slope of a point on the reactor wall with respect to the ground surface(°)
I_{refl}	Ground reflected diffuse light(μmol m^{-2} s^{-1})	γ_S	Solar azimuth angle(°)
K_1	Fitted model parameters	δ	solar declination(°)
K_2	Fitted model parameters	θ_z	zenith angle(°)
K_i	Growth model parameters for *Chlorella* sp. 11_H5	μ_{max}	Maximum specific growth rate(h^{-1})

K_s	Growth model parameters for *Chlorella* sp. 11_H5	$\overline{\mu}$	Average specific growth rate(h^{-1})
K_t	Daily clearness index	ρ	Ground reflectivity
L	Spacing distance between reactors in east-west or north-south direction (edge to edge)(m)	ρ_w	Density of culture broth (kg m^{-3})
L/H	Spacing distance to height ratio(m m^{-1})	σ	Extinction coefficient (m^2 g^{-1})
L'	Average distance between the columns(m)	Φ	Latitude of location(°)
n	Day number in year, 1st January is 1	φ	p
n1	Refractive indexes of air	ω	Solar hour angle(°)
n2	Refractive indexes of water	ω_i	angular displacement from east of the projection of beam radiation on the horizontal plane(°)
P_{areal}	Annual average areal productivity (t dry weight ha^{-1} y^{-1})	ω_s	Sunset hour angle(°)
P_{Direct}	Light path of direct light in reactor (m)		

1. Introduction

Solar driven microalgae biotechnologies offer sustainable solutions to improve global food, water and fuel security, and supply a wide range of chemical feedstocks (e.g. omega-3 fatty acids, antioxidants and recombinant proteins) [1]. To efficiently produce algal biomass with low cost, a diverse array of microalgae system designs is being developed internationally [2, 3]. Commercial systems development has been impeded by limited data on climate related algae responses, the identification of optimal production conditions (e.g. nutrients, light, temperature) [4], as well as the high cost of pilot and demonstration scale systems testing. Detailed models can provide powerful tools for the optimisation of system design, to de-risk scale up and identify the most promising business models. Such predictive models have been developed to evaluate large-scale flat panel and tubular photobioreactor (PBR) systems [5, 6], but, to our knowledge, not large scale cylindrical (or 'vertical column') photobioreactor arrays (Fig.1). Cylindrical PBRs are being used widely to culture microalgae for aquaculture feeds [7], for wastewater treatment [8], to capture flue gas CO_2 [9], and for biofuel production [10] as they are compact, modular, easy to operate and reportedly have excellent gas-liquid transfer performance [11].

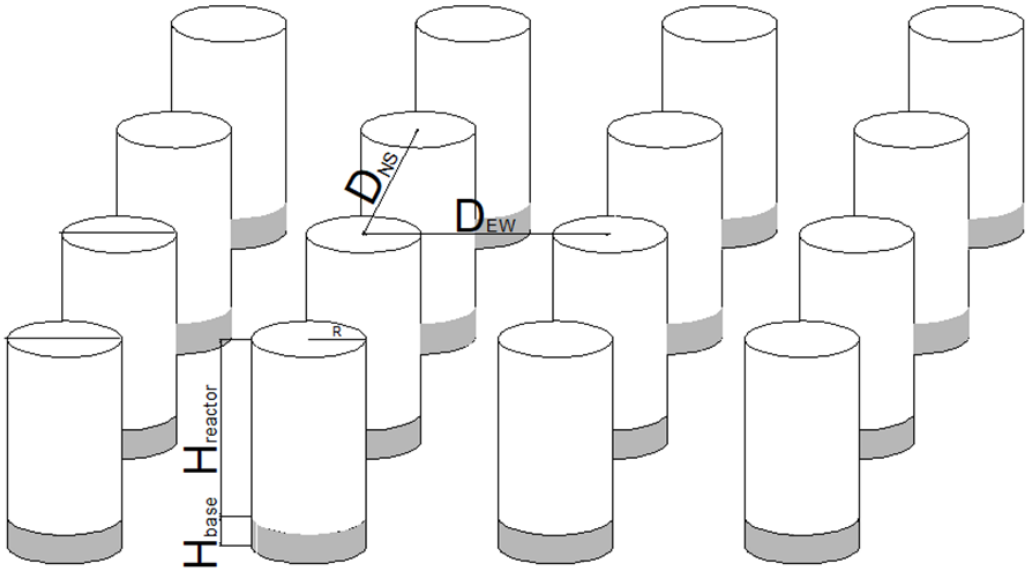

Fig.1. Schematic of an array of vertical cylindrical PBRs (D_{EW} is distance between neighboring reactor in east-west direction (center to center), D_{NS} *is the* distance between neighboring reactor in south-north direction (center to center), R is the reactor diameter, $H_{reactor}$ is the height of photobioreactor, H_{base} is the height of base).

Many experimental or modelling studies of microalgae cultivation in cylindrical PBR systems have focused on single isolated reactors [12-17]. However, in a commercial facility, PBRs are positioned in large 2D arrays which increasingly shade each other as their height increases and the distance between them is reduced. Systems optimisation therefore not only requires modelling of individual PBR performance (e.g. in response incident light intensity/direction, culture density, column diameter and temperature,) but also complex modelling of the temporal and special distribution of both light and temperature, of the arrayed PBRs.

Here, we present a comprehensive model capable of analysing light and temperature dependent algal productivities under various designs of large scale 2D arrays of cylindrical PBRs.

The model predicts changes in light regime and temperature simultaneously, by calculating the effects of solar shading between columns, reflected ground radiation,

and the vertical gradient of diffuse radiation around PBRs (i.e. the 'canyon effect') on ambient light and culture temperature, and their effects on algae productivity. The model supports system analysis and optimisation based on PBR diameter, height and spacing distance, as well as biomass concentration and cultivation modes (batch and continuous), to estimate their effects on volumetric and areal biomass productivity. For simulations, we chose three species of the green chlorophyte *Chlorella*, as they are industrially relevant, well characterised and have some of the highest reported growth rates in the literature [14, 18]

2. Model description

2.1 Simulation method

Microalgae growth rates are dependent on the production parameters: light, temperature, nutrients, pH, CO_2, and predation [19-20]. The simulation presented here is focused on the modelling of growth as a function of light and temperature, assuming that all other parameters are non-limiting. The overall microalgae biomass predictive model structure is shown in Fig.2. First, the amount and distribution of hourly solar radiation, including direct light, diffuse and ground reflected light, impinging upon the surface of cylindrical reactors is calculated based on typical daily global horizontal radiation inputs, using formulas in Appendix A. Within large scale cylindrical photobioreactor arrays (e.g. 100 x 100 vertical cylindrical PBRs), direct incident light can be blocked by neighboring PBRs to an extent, determined by the time of day, PBR spacing, height, diameter and position [5-6]. Diffuse light intensity is gradated in the space between PBRs and parallel to their vertical axis (i.e. the 'canyon effect'); this diffuse light gradation is also influenced by the light reflected from the ground [21-22].

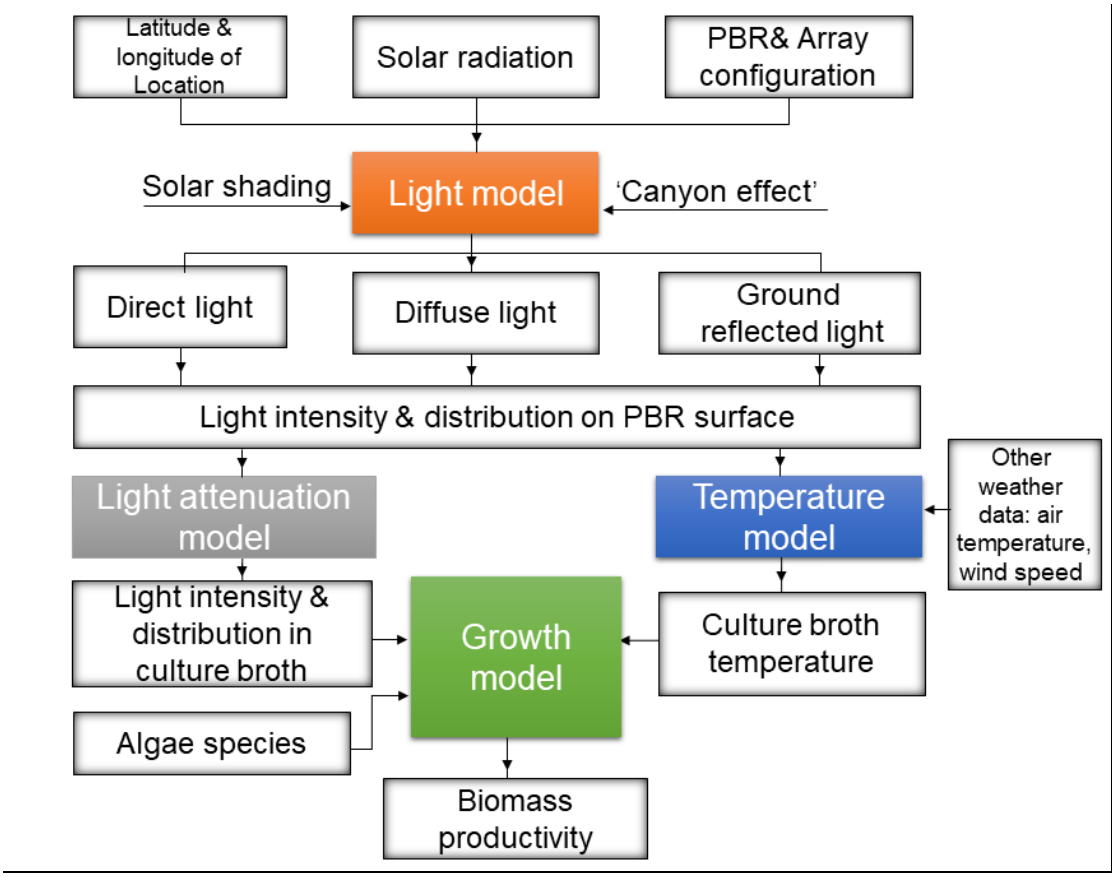

Fig.2. Schematic of microalgae biomass calculation scheme.

Then, local light intensity at any point inside the cylindrical PBR is calculated using a light attenuation model (Lambert–Beer's law), which considers the biomass density of the culture, the light path, and the optical properties of the cell. The local light intensity contributed from direct light, and those contributed from diffuse light and ground reflected light is calculated respectively due to different light paths for direct light, and diffuse light and ground reflected light. Light path for direct light is dependent on sun location (e.g. solar zenith angle, and azimuth angle). The light path of diffuse and ground reflected light is not dependent on sun location, and assumed to be perpendicular to the reactor wall [6]. The incident light transmitted into the culture medium is subject to reflective and absorptive losses at the reactor wall interface [21], which is also considered in the model. The sum of local light intensity sourced from direct light, and those from diffuse and ground reflect light as the total local light

intensity is input to algal growth model to calculation the specific growth rate, together with culture temperature. The culture liquid's temperature is estimated from the solar radiation received by each PBR, together with other weather data such as air temperature obtained from EnergyPlus (https://energyplus.net/), via a modified model based on that of Bechet et al. [23]. The culture is considered well mixed and thus the temperature is assumed to be homogenous in the whole PBR. Using these models the microalgae biomass productivity influenced by light and temperature factors are derived [19, 24]. The light, temperature and growth model equations are detailed in the Appendix A, B and C, respectively. The models and simulations were developed and performed in Matlab software (Mathworks). All equations of light model are algebraic equations; main equations of temperature and growth model are ordinary differential equations. Thus, a discretization method is used to process the model. For balancing the compute load and simulation accuracy, the time interval is set to half hour, and the PBR height is divided into 20 sections from bottom to top with horizontal cross-sections of the PBR divided into 10 disk-shaped segments from outside to inside and circumference divided into 120 segments (i.e. each segment corresponding to 3^{o}). The area-averaged algal specific growth rate is obtained at each horizontal cross-section. Then, these specific growth rates are averaged to represent the overall specific growth rate inside PBR.

2.2 Scenario designs

A range of scenarios were analysed to investigate variable effects on biomass productivity, relating to reactor configuration, operational conditions and temperature control strategies (Table 1). Fig.1 shows a modelled large-scale microalgae cultivation plant consisting of regularly spaced cylindrical PBRs. The arrayed PBRs were assumed

to be arranged uniformly and in parallel in both the east-west direction and the north-south direction. A center-to-center distance between neighboring reactor in east-west direction (D_{EW}) is equivalent to center-to-center distance between neighboring reactor in north-south direction (D_{NS}). The reactor configuration variables analysed included: reactor diameter, D (m), reactor height (including base), H (m) and the spacing distance between reactors, L (m). The operation variables included operating regime (batch or continuous), and operating dry weight biomass concentration, C_x (g L^{-1}). The annual average volumetric or areal biomass productivity (P_{vol}, g L^{-1} d^{-1} and P_{areal} t ha^{-1} y^{-1} respectively) were used to evaluate the system performance. The typical PBR located in the middle of the arrayed PBRs system was choosen for model simulation. A few PBRs along or near the sides of the system, obtaining more light and less shading, was not considered as is negligible to the size of the facility.

The cultivation location modelled for algae production was Brisbane, Australia, which has a sub-tropical climate, well suited to microalgae production. In the continuous culture mode, steady-state operating biomass concentrations ranging from 0.3–1.5 g L^{-1} were tested, where the dilution rate is assumed as equal to the specific growth rate. The biomass concentration inside the PBR is assumed to be controlled under a continuous regime during daylight hours over the year. This can be achieved by regulating the dilution rate by feedback on deviations of the biomass concentration, using an online turbidity metre. Thus, the net biomass productivity is equal to biomass obtained during daytime minus the biomass loss during night. For batch mode, the harvest was carried out at the end of microalgae cultivation period without fresh medium added during the process. The initial biomass concentration of the culture and cultivation period was set to 0.15 g L^{-1} and 7 days, respectively. Biomass loss due to dark respiration was modelled to be continuous and at a constant basal rate throughout

the night, irrespective of photosynthetic activity during the day [12]. The productivity during the day and net productivity over 24 hours were compared to assess the effect of respiration losses.

Three species of the chlorophyte *Chlorella* were selected for simulation: *C. vulgaris* [24], *C. pyrenoidosa* [25] and *Chlorella* sp. 11_H5 [3]. Each species has different reported photosynthetic characteristics and light absorption coefficients [3, 19, 24-26]. Two temperature control strategies were tested: 1) 'Fixed': the specific temperature, T (^{o}C) of each strain's appropriate or optimal temperature, T_{app} or T_{opt}; or 2) 'Variable': fluctuating temperature with cooling to T_{app} or T_{opt}, if T exceeded this threshold (for *C. vulgaris* and *C. Pyrenoidosa* only). The heat exchanger is equipped inside the PBR to control the culture broth temperature according to temperature control strategies, using hot water heated by electrical device or cold water from deeper sea. The light transfer affected by the heat exchanger inside the PBR is neglected. For simulation under a fixed temperature regime, algal growth was a function of light; while the upper limit temperature was used when the predicted temperature of PBR exceeded the upper limit for the variable temperature situation. The heat energy (hot water) was supplied to maintain at a fixed temperature when the net heat flow is negative for reactor (e.g. at low air temperature condition in the morning); while heat energy was removed from reactor by means of cold water when reactor temperature was higher than the upper limit temperature (e.g. too much solar radiation obtained at the noon). These heat energy supplied and removed was calculated and compared for the two different temperature control strategies (fixed or maintained under a maximum threshold). The temperature control is only conducted during daytime, without controlling night condition for microalgae culture. The mixture gas of air and CO_2 with 0.35 vvm flow rate is achieved inside PBR to provide mixing and carbon source. The complete mixing is assumed

inside PBR. All factors except light and temperature, such as mixing condition, gas condition, pH etc., are non-limiting factors for microalgae growth simulation.

Table 1. Decision variables for algal biomass productivity simulations (T_{app} is strain's appropriate temperature for growth, T_{opt} is strain's optimal temperature for growth, D is reactor diameter, *L is* spacing distance between reactors (edge to edge), H_{PBR} is reactor height, H_{base} is base height, *H* is the total height, *L/H* is spacing distance to height ratio, C_x is biomass concentration for continuous cultivation, $C_{x,initial}$ is initial biomass concentration for batch cultivation).

Decision variable	Value(s) used in model simulations
Location:	Brisbane (27°50'S, 153°03'E)
Algae Species:	*Chlorella vulgaris* (T_{app}[1] = 29.3 ºC) *Chlorella pyrenoidosa,* (T_{opt}[2] = 38.7 ºC) *Chlorella* sp. *11_H5* (T_{opt} = 25 ºC)
Reactor type:	Cylindrical PBR
Reactor diameter, *D* (m):	0.1, 0.15, 0.2, 0.3
Spacing distance between reactors (edge to edge), *L* (m):	0.05–1.8
Reactor height, H_{PBR} (m):	1.0, 1.5, 2.0, 3.0
Base height, H_{base}, (m):	0.25
Height, *H* (m):	1.25, 1.75, 2.25, 3.25
Spacing distance to height ratio, *L/H* (m m^{-1})	0.028 – 1
Operating regime:	• Continuous • Batch
Operating dry weight biomass concentration, C_x (g L^{-1})	0.3, 0.5, 1, 1.5 (continuous) 0.15 ($C_{x,initial}$, batch)
Temperature control regime:	• 'Fixed' at species-specific T_{opt} • 'Variable' dynamic temperature with cooling above T_{opt}.

[1]: T_{app} is the appropriate temperature of microalgae strain. Microalgae performs overall high growth rate over range of light intensity. However, appropriate temperature is not the optimal one as the optimal temperature is dependent on light intensity for this strain (as shown in Fig.C1in Appendix).

[2]: T_{opt} is the optimal temperature of microalgae strain. Microalgae have the highest

growth rate at this temperature regardless of light intensity for the strain (as shown in Fig.C1in Appendix).

3. Simulation results and discussion

3.1 Light distribution profiles of parallel cylindrical PBRs

Fig.3 shows the light distribution within vertical and horizontal cross-sections of parallel positioned cylindrical PBRs at different times of the day (08:00–17:00) on January 1 (Summer), in Brisbane at two different PBR diameters (A. D = 0.1 m; B. D = 0.15 m diameter). For both cases, the spacing distance between reactors (edge to edge) was 0.4 m in both east-west and north-south direction and the PBR height, H_{PBR}, was 1.5 m. The steep light gradient through the PBR culture is evident in both vertical and horizontal directions of PBRs. Along the vertical axis over the day, extremely high irradiance occurs close to the PBR surface facing the sun. Shading by neighbouring reactors, however, blocks this direct irradiance to variable portions of the lower PBR depending on the sun's angle at a given time.

Larger diameter PBRs (e.g. 0.15 m) relatively have a higher proportion of the culture exposed to the dark zone (<10 μ mol m^{-2} s^{-1}) in which respiratory losses exceed photosynthetic gains. Additionally, they are more shaded by surrounding PBRs, compared to small diameter PBRs (e.g. 0.1 m) because of the higher reactor to areal footprint ratio. Reduced shading, together with an improved light distribution of the smaller diameter PBRs results in a higher fraction of the culture being in the optimal light range (~50-150 μmol m^{-2} s^{-1}). The smaller 0.1 m diameter reactors, with their lower thermal mass, and higher surface area to volume ratio, exhibited only slightly higher temperatures (23.97 ºC – 33.52 ºC: Δ 9.55ºC) over the day than their larger diameter counterpart (22.43 ºC – 32.40 ºC: Δ 9.97ºC). The maximum temperature of

the culture liquid exceeded the growth threshold for *C. vulgaris*, but not for *C. pyrenoidosa* (Table 1).

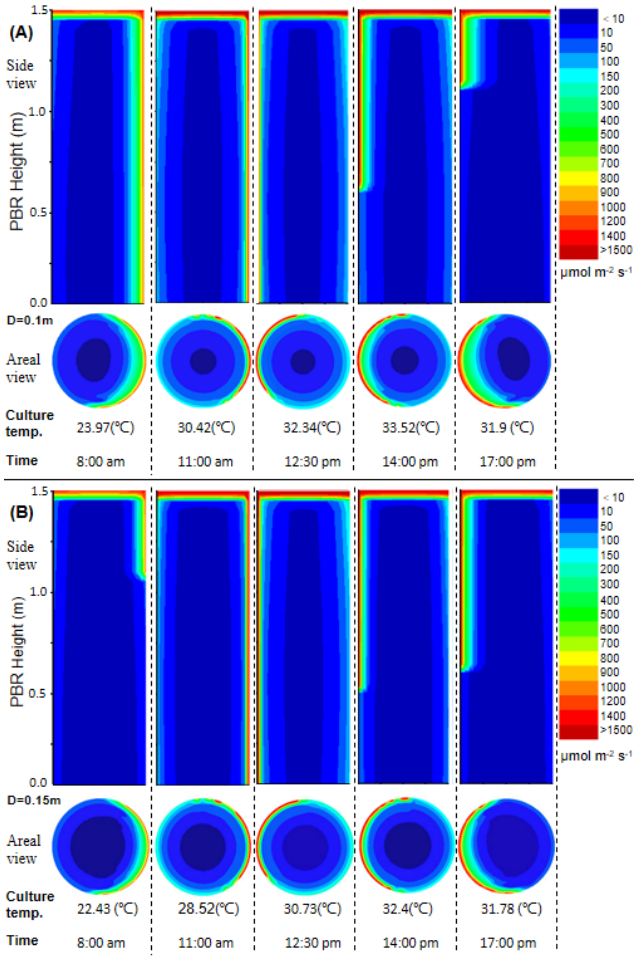

Fig.3. Light intensity distribution over time in a 1.5 m high cylindrical PBR with a spacing distance of 0.4 m and a biomass concentration of 0.5 g L^{-1} (*C. vulgaris*) with diameter 0.1m (A) and 0.15m (B). Light intensity within the PBRs is colour coded from blue (<10 μmol m^{-2} s^{-1}) to red (>1500 μmol m^{-2} s^{-1}). The vertical PBR cross sections (top) are oriented west (left) –east (right). The horizontal cross sections were taken at a height of 1.25 m above the bottom of PBR. The change in temperature over time is also indicated. D is the diameter of reactor. Culture temp. is the temperature of culture broth.

3.2 Comparison of biomass productivity in arrayed PBRs and a single PBR

With the light and temperature profiles established, the predicted annual averaged volumetric dry biomass productivity of a single PBR was compared with that of an

array of multiple PBRs under a variable temperature regime (Fig 4). P_{vol} of parallel PBRs (solid markers) was lower than that of a single PBR (open markers) because of a reduction of total irradiance from both shading effects on direct light, as well an increased 'canyon effect' , that lower levels of diffuse and ground reflected light [5, 6]. The P_{vol} of the arrayed PBRs (Fig.4, solid markers) increased with *L/H* in a hyperbolic manner, approaching that of a single PBR (Fig.4 open markers) as the distance between PBRs was increased. For example, for the lowest operating biomass concentration (blue line; C_x = 0.3 g L^{-1}), the ratio of P_{vol} of arrayed reactors to single reactor rises from 9.21 % to 80.51 %.

Fig. 4A and B compare the large difference in P_{vol} of different operating biomass concentrations on productivity without and with consideration for respiratory biomass loss during the night respectively. During the day, increasing the operating biomass concentration, yields great improvements in P_{vol} (Fig. 4A). These gains, however, are mostly lost at night due to the higher volumetric respiration loads that accompany increased cell densities (Fig. 4B). In fact, at low *L/H*, high C_x can cause negative net P_{vol}, whilst even for unshaded PBRs (open markers), a C_x of 1 g L^{-1} had slightly better P_{vol} than at 1.5 g L^{-1} for a diameter of 0.15 m. Moreover, the ratio between P_{vol} in array PBRs at 1 m to single PBRs was slightly better without respiration compared to with respiration for all biomass concentrations, highlighting that respiration loss is higher in shaded reactors.

These results highlight the importance of ensuring that an optimal C_x range is maintained.

In summary, the optimisation of bioreactor spacing, biomass concentration and the balance between photosynthetic gain and respiratory losses are all important considerations for high efficiency photoautotrophic microalgae cultivation [27]. High

biomass losses can occur at night with increasing cell density and even result in negative growth rates, if these are higher than day time productivity (e.g. when distance between PBRs is small).

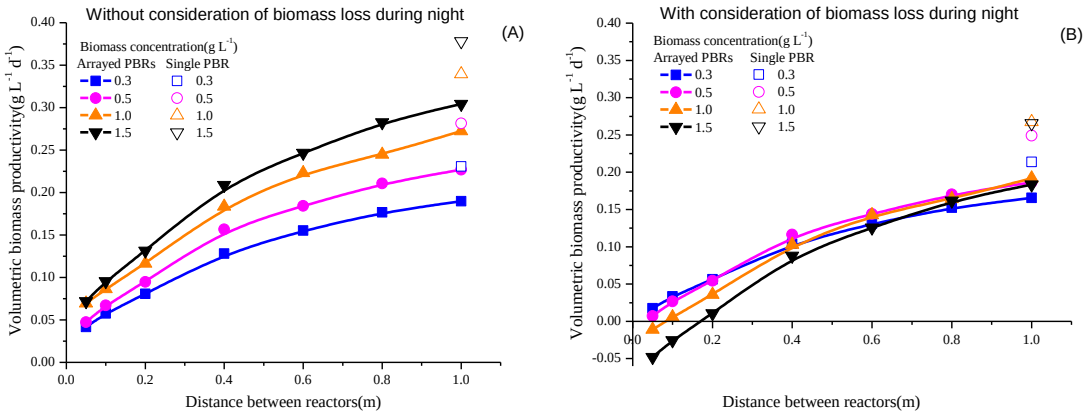

Fig.4 The volumetric productivity of C. *vulgaris* in a single and arrayed PBRs (A) with and (B) without consideration of respiratory biomass loss during night (reactor diameter 0.15 m and height 1.5 m)

3.3 Effect of PBR diameter, spacing distance and biomass concentration on the net productivity of *C. vulgaris*

The next analysis compares the complex interplay of systems design parameters including: PBR diameter, spacing distance to height ratio and biomass concentration on the net productivity of C. *vulgaris* under continuous culture, under a dynamic temperature regime.

Fig. 5 showed that conditions delivering the highest *volumetric* biomass productivity (left panels) are not the same as those realising the highest *areal* biomass productivity (right panels).

As the spacing distance increased, so too did the P_{vol} in each PBR. In parallel, however, the total volume of culture (Vol, m^3 ha-1, left panels, green dashed line) declines due to the lower number of PBRs per unit area. This results in a maximum P_{areal} that is a trade-off between P_{vol} and number of PBRs, such that Pareal rises sharply at a low L/H due

to a rapid increase in P_{vol}, before decreasing as the total culture volume is reduced (Fig.5). A similar phenomenon was also reported for flat panel and tubular PBRs [5, 6]. The highest annual areal biomass productivity of 1.5 m high cylindrical PBRs was calculated to be obtained using 0.15 m diameter systems, aligned along a 0.1 m spacing grid and operated at culture density of 0.3 g L^{-1} (Fig.4B blue line; P_{areal} = 51.7 t ha yr^{-1}).

The effect of PBR diameter shows a dramatic effect on P_{vol}. At the highest *L/H* analysed, the smallest diameter (0.1 m) showed an approximate 2- and 3-fold higher P_{vol} than that at 0.2 m and 0.3 m, and was able to sustain higher biomass concentrations and lower total volumes. Remarkably, the results were almost the opposite on an areal basis; here the highest P_{areal} was favoured at higher diameters but dilute biomass concentrations.

These results illustrate the complexity of optimizing the design of 2D arrays of closed PBR. Techno-economic analyses have identified that harvest costs attributed to load volumes and freshwater requirements as significant factors that add to the cost of microalgae production in several locations [37]. For these reasons, maximising P_{vol} is likely to improve economic feasibility. Furthermore, it reduces the number of PBRs required and their associated costs. However, for locations where land is scarce (e.g. China, Japan or parts of Europe), the cost and availability of land may be a limiting factor and therefore P_{areal} may have higher importance.

In summary, Fig.5 shows that:

- lower density cultures (e.g. 0.3 g L^{-1}, blue line) tend to yield higher *areal* productivities than high density cultures (e.g. 1.5 g L^{-1}, black line)
- areal biomass productivity is more sensitive to change as PBR spacing is reduced towards 0 m, than when it is increased towards infinity.
- maximum productivity is achieved at highest light to volume ratios on a

volumetric basis; but high culture volume and low light intensity on an areal basis.

- The fact that small errors in optimal spacing can dramatically decrease areal biomass productivity (Fig.4) highlight the benefit of detailed array modelling.

In conclusion, these findings are critical to couple with location-specific techno-economic and life cycle analyses to guide optimal facilities design.

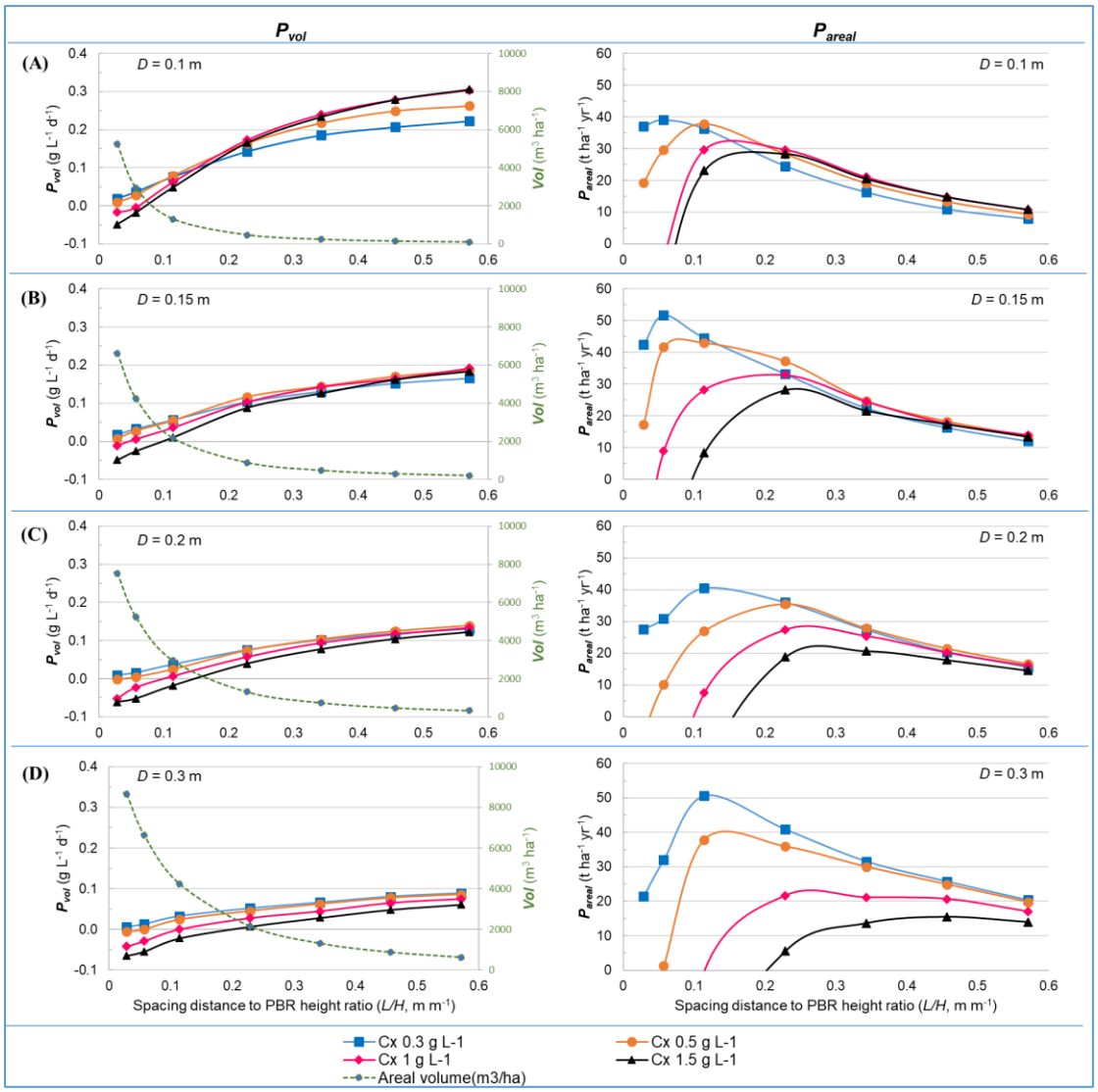

Fig. 5. Comparison of annual averaged biomass productivities on a volumetric (P_{vol}, left panels) and areal (P_{areal}, right panels) basis for *C. vulgaris* in arrayed 1.5 m high cylindrical PBRs with differing diameters (A: 0.1m, B: 0.15m, C: 0.2m and D: 0.3 m diameters) and spacing to PBR height ratios (0.02–0.6). The dashed lines show the rapid drop of areal PBR volume as function of increased PBR spacing to height ratios. Cultivated under continuous harvest and a variable temperature regime. P_{vol} is annual average volumetric productivity. P_{areal} is the annual average

areal productivity. D is the reactor diameter. L/H is the spacing distance to height ratio.

3.4 Effect of reactor height on biomass productivity

Fig.6 shows the performance of arrayed PBRs with various reactor heights. It was found that P_{vol} increased inversely to reactor height at low L/H conditions. As L/H increased, the total culture volume was reduced for larger reactors. Thus for all cases, the P_{areal} was higher for the same L/H ratio at low PBR height. However, on the basis of absolute spacing distance between reactors, P_{areal} increased as L increased for higher PBRs due to the larger volume.

It should be noted that the model does not account for changes in reactor pressure and mixing constraints that may occur for very high reactors. It is designed to enable rapid optimisation of spacing distances for PBR with different heights as a function of light and temperature.

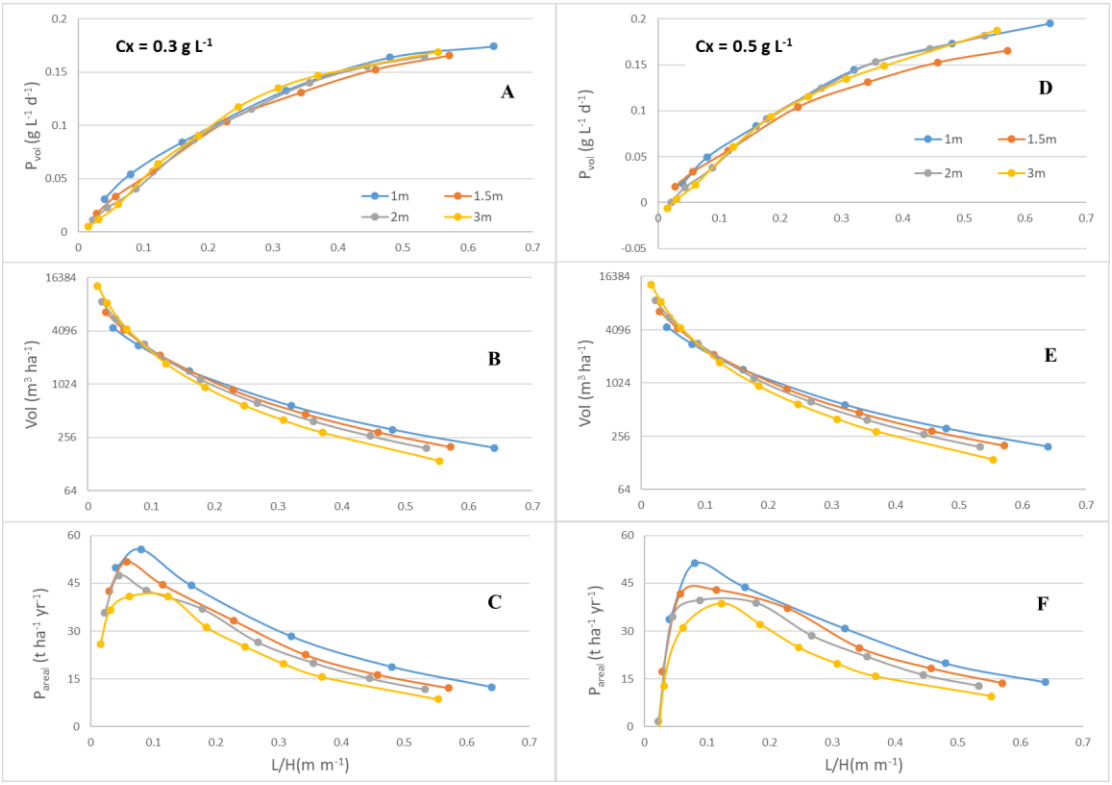

Fig. 6. Relationship between PBR height and productivity. A & D shows P_{vol} are very similar for each PBR height as a function of spacing distance to height ratio. However, the total culture volume

for taller PBRs decreases more than shorter PBRs. Thus, P_{areal} is higher at all L/H ratios for shorter PBRs. P_{vol} is annual average volumetric productivity. P_{areal} is the annual average areal productivity. C_x is the biomass concentration. *L/H* is the spacing distance to height ratio. *Vol.* is the volume of total photobioreactor per hectare.

3.5 A simple relationship between biomass productivity and configuration variables supports systems optimisation

The complexity of developing the full model presented here and testing the interaction of its many variables is computationally expensive and time consuming. We therefore analysed whether a simple relationship of biomass productivity in a single PBR could be derived to PBRs in an arrayed configuration. It was found that much of the variation in biomass productivity related to the operating concentration and PBR diameter for *single*, *unshaded* PBRs. Indeed, normalising the ratio between the P_{vol} in a PBR *within an array*, versus a *single, unshaded* PBR yielded almost the same proportions for each D and C_x at a given light to height ratio (Fig. 7).

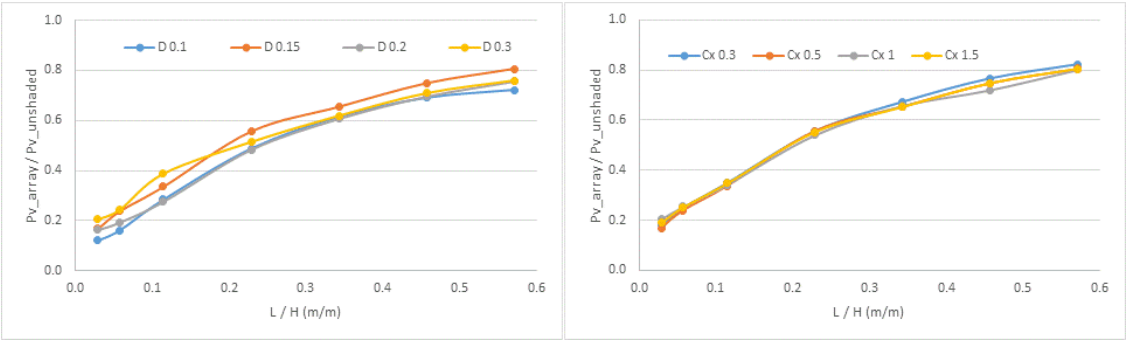

Fig.7. Ratio of biomass productivity of arrayed PBRs to a single PBR (left: under different diameters conditions at biomass concentration 0.5 g L^{-1}; right: under different biomass concentrations with diameter 0.15m). *L/H* is the spacing distance to height ratio. $P_{v\_array}/P_{v\_unshaded}$ is the ratio of annual average volumetric productivity of arrayed PBRs to that of a single, unshaded PBR.

Thus, knowing only the P_{vol} of a single isolated PBR and L/H, the relationship between

volumetric biomass productivity and configuration variables almost satisfy Equations (1) and (2) both without, and with nightly biomass losses through respiration, respectively,

$$P_{vol-light} = P_{vol_s} \cdot K_1 \left(\frac{L}{H}\right)^{K_2} \quad \text{Eq. 1}$$

$$P_{vol} = P_{vol_s} \cdot K_1 \left(\frac{L}{H}\right)^{K_2} - C_x \cdot (1 - \exp(-r_d \cdot t_{night})) \quad \text{Eq. 2}$$

Where, $P_{vol\text{-}light}$ is the volumetric biomass productivity of arrayed PBRs during the light period of day (g L^{-1} d^{-1}) without nightly biomass loss and P_{vol_s} is the biomass productivity of a single, isolated PBR during the light period of day (g L^{-1} d^{-1}); r_d is the specific death rate during night (h^{-1}), t_{night} is the time during night (h).

K_1 and K_2 are fitted model parameters, where:

$K_1 = 1.09$ and $K_2 = 0.528$

The model fit was $R^2 = 0.9799$ with most of the residuals occurring at extremely small *L/H* ratios.

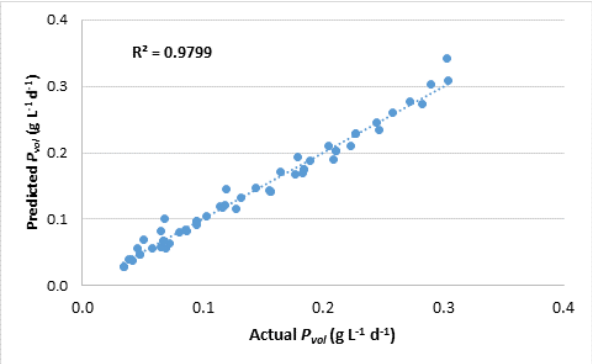

Fig. 8. Comparison of actual modelled data (x-axis) with estimated data using Eq.2 (P_{vol} is annual average volumetric productivity).

Fig.8 shows Eq. (2) fit the biomass productivity data well with high R^2 ($\geqslant$0.9799) for all biomass concentrations and reactor diameters considered. The fitted model shows that different reactor heights can achieve virtually the same volumetric biomass productivities providing the spacing distance: reactor height (L/H) ratio is kept constant

(as shown in Fig. 6).

3.6 Comparison of performance between different algae species

Algae production strains exhibit species-specific differences in biomass productivity (Fig.9). Under the same configuration condition (reactor diameter 0.15 m; height 1.5 m) and biomass concentration (0.3 g L^{-1}), the predicted maximum annual biomass production of *C. vulgaris* is ~50 t ha^{-1} y^{-1}. This is 2.5 fold higher that of *C. pyrenoidosa* (~20 t ha^{-1} y^{-1}), but half that of *C. sp 11_H5* (~100 t ha^{-1} y^{-1}). It should be noted that typical open pond systems operated at 20g m^{-2} d^{-1} correspond to annual productivities of 70 t ha^{-1} y^{-1} (i.e. 365 days per year, 10,000 m^2 per hectare). The large production differences among species is mainly attributed to their different photosynthetic growth characteristics (Appendix C, Fig. C.1). In particular, the specific growth rates of *C. vulgaris* and *C. pyrenoidosa* are much lower than that of *Chlorella* sp. 11_H5 at the same incident light. Significant differences in biomass production between these algae species are highlighted by the daily average biomass productivities (Fig.10). For all strains, the daily average biomass productivity during Australia's winter (mid-plot) is much lower than in summer, but this trend is more extreme for *Chlorella* sp. 11_H5. It is also found that the optimal PBR spacing distance for these three species differ because of their growth characteristics in response to light and temperature. In summary, species specific system design is important to achieve optimal biomass productivities.

The results show that biomass productivity would significantly increase if respiration losses during the night could be reduced or eliminated. The predicted maximum biomass productivities with zero biomass loss (~100 t ha^{-1} y^{-1} for *C. vulgaris*, ~40 t ha^{-1} y^{-1} for *C. pyrenoidosa*, and ~180 t ha^{-1} y^{-1} for *C.*sp. 11_H5*)* were almost two-fold higher than those exhibiting biomass loss during the night (~50 t ha^{-1} y^{-1} for *C. vulgaris*,

~20 t ha^{-1} y^{-1} for *C .pyrenoidosa*, and ~110 t ha^{-1} y^{-1} for *C.* sp. 11_H5). Comparatively, the biomass productivities have been reported to be ~36-189 t ha^{-1} y^{-1} for flat panel and tubular PBRs obtained by experiment or model simulation [5, 6, 28-30]. These large differences in biomass productivities reported for flat panel and tubular PBRs, are similar to the findings presented here for cylindrical PBR by means of model simulation, and can be explained by the different configurations and layouts of PBRs employed, different strains used, facility location, as well as whether respiration dependent losses during the night are considered [5, 6].

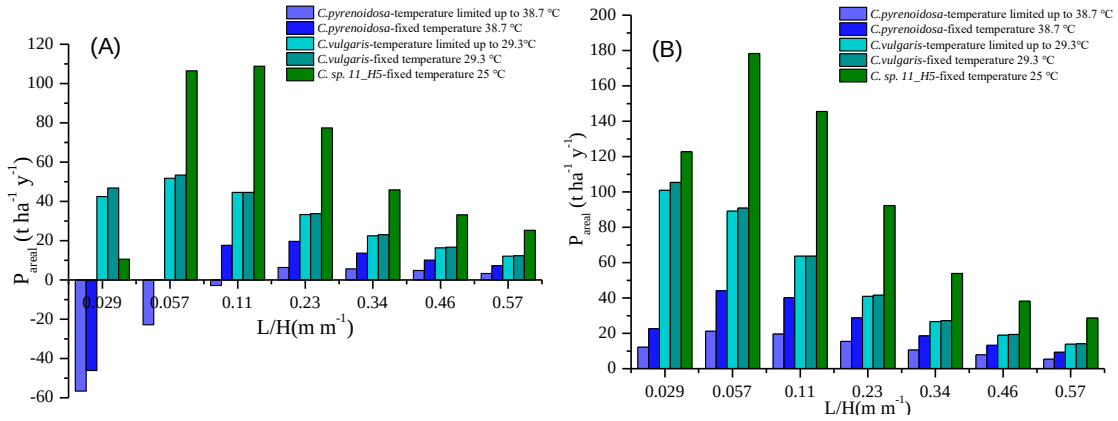

Fig.9 Comparison of biomass productivity of different algae species: A) accounting for biomass loss during night; and B) without accounting for biomass loss during night (reactor diameter 0.15 m, height 1.5 m, biomass concentration 0.3 g L^{-1}, and continuous culture). P*$_{areal}$* is the annual average areal productivity. *L/H* is the spacing distance to height ratio.

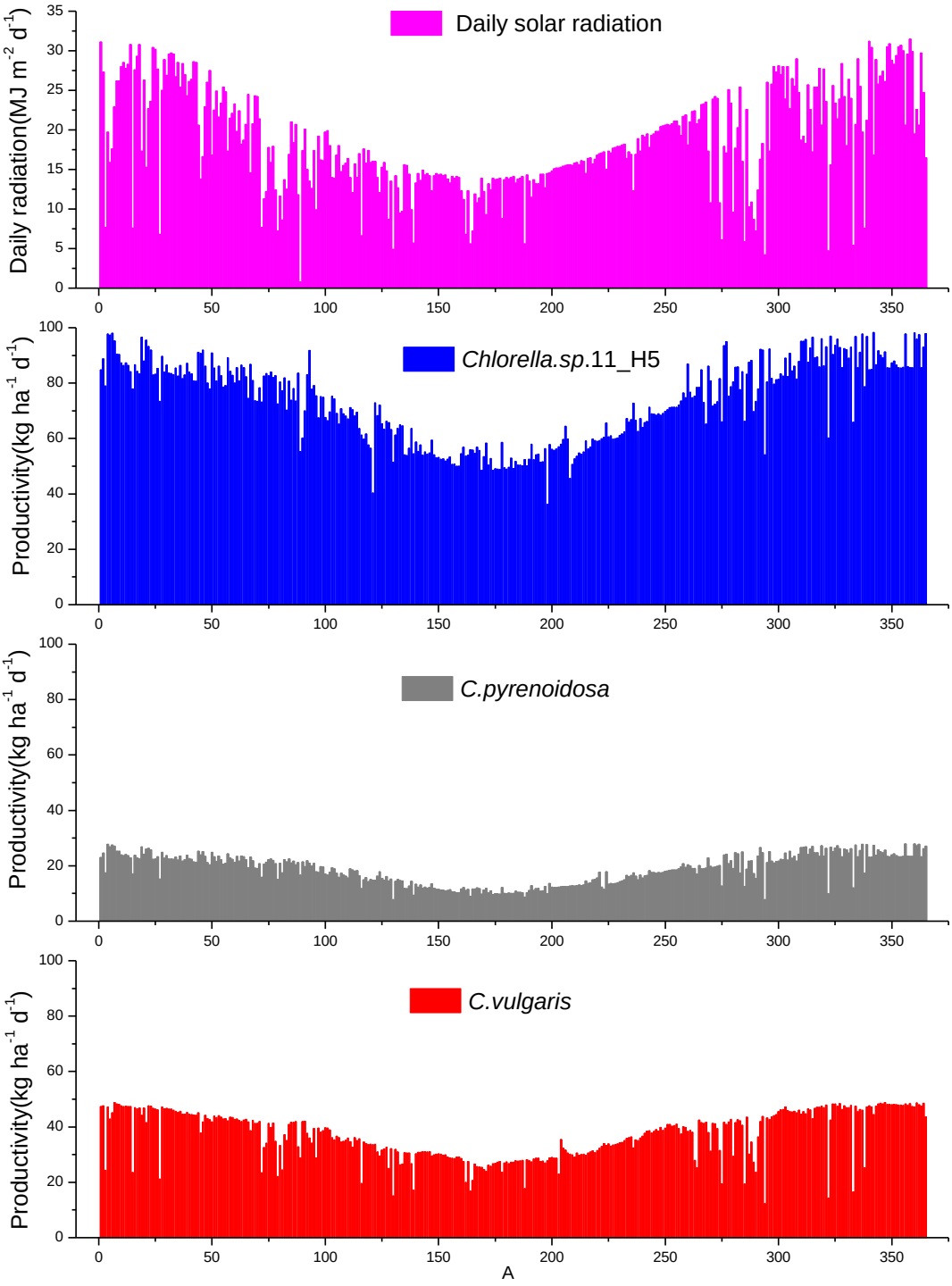

Fig.10 Comparison of daily average biomass productivity of different algae species (reactor diameter 0.15 m, height 1.5 m, distance between reactors 1 m, and biomass concentration 0.5 g L^{-1}).

3.7 Continuous and batch cultivation

For operation under continuous or batch cultivation, the preferred harvest regime was

dependent on the algal species and temperature regime. For instance, the P_{areal} of *Chlorella sp.* 11_H5 using continuous mode (106.5 t ha^{-1} y^{-1}) was much greater than that using batch mode (71.1 t ha^{-1} y^{-1}) under a fixed temperature, spacing distance of 0.1 m and biomass concentration of 0.3 g L^{-1} (Table 2). However, for *C. vulgaris*, at these same conditions, the P_{areal} using continuous mode (53.4 t ha^{-1} y^{-1}) was only slightly higher than that using batch mode (50.7 t ha^{-1} y^{-1}), and for *C. pyrenoidosa* similar photosynthetic gains and respiration loss equated to zero net biomass production of occurred under continuous mode, while batch mode produced an estimated 14.1 t ha^{-1} y^{-1}. The P_{areal} of *C. sp* 11_H5 and *C. vulgaris* with continuous mode were estimated to be lower than those produced using batch mode when the biomass concentration was increased to 0.5 g L^{-1}. In summary, these results indicate that the advantage of continuous cultivation is only found when the optimum algae concentration together with the spacing distance to height ratio (*L/H*) is used.

Table 2. Comparison of batch and continuous cultivation model under different temperature control strategies in arrayed PBRs with 0.15 m diameter and 1.5 m height. *L/H* is the spacing distance to height ratio.

Species	Areal productivity of continuous cultivation [a] (t ha^{-1} y^{-1})	Areal productivity of batch cultivation [b] (t ha^{-1} y^{-1})	Heat energy supplied (kJ ha^{-1} y^{-1})	Heat energy removed (kJ ha^{-1} y^{-1})	L/H (m m^{-1})	Temperature control strategy during daytime
C.sp. 11_H5	106.5 (2.9[e])	71.1	1.60E+11	5.15E+10	0.06	Fixed 25 ℃
C.sp. 11_H5	77.5	46.9	2.77E+10	1.92E+10	0.23	Fixed 25 ℃
C.vulgaris	53.4 (46.3[e])	50.7	3.17E+11	6.44E+09	0.06	Fixed 29.3 ℃
C.vulgaris	51.7	48.7	0	3.47E+09	0.06	Limited up to 29.3℃
C.vulgaris	33.8	33.3	5.52E+10	4.82E+09	0.23	Fixed 29.3 ℃
C.vulgaris	33.2	32.9	0	3.55E+09	0.23	Limited up to 29.3℃
C.pyrenoidosa	0 [c]	14.1	6.70E+11	6.84E+06	0.06	Fixed 38.7 ℃
C.pyrenoidosa	-22.8	-3.4	0	0 [d]	0.06	Limited up to 38.7℃
C.pyrenoidosa	19.7	16.3	1.25E+11	4.98E+07	0.23	fixed 38.7℃

C.pyrenoidosa	6.3	6.6	0	0 [d]	0.23	Limited up to 38.7℃
C.pyrenoidosa	5.7	5.9	0	7.27E+06	0.34	Limited up to 38.7℃

[a]: Continuous cultivation with biomass concentration 0.3g L^{-1} including biomass loss during night

[b]: Batch cultivation with initial biomass concentration 0.15g L^{-1} including biomass loss during night

[c]: The amount of biomass production during daytime is equal to that loss during night

[d]: The maximum temperature of reactor is below 38.7 ℃

[e]: Continuous cultivation with biomass concentration 0.5 g L^{-1} including biomass loss during night

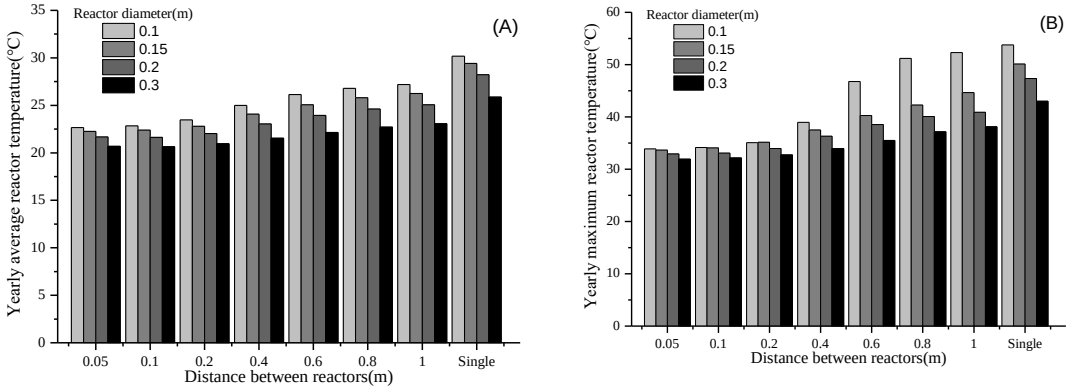

Fig.11 The predicted annual average (A) and maximum (B) culture temperature at daytime with different PBR configurations. The model predicted that culture temperature in arrayed PBRs increased with increased spacing distance. The difference between the yearly average and maximum temperatures suggests that PBRs with larger diameters (0.3m, black) exhibit less variation and lower overall temperatures than PBRs of lower diameters, particularly at larger spacing distances.

3.8 Temperature control effect

Temperature is one of the most important factors influencing the algae growth rate (Table 2). Two temperature control strategies include: maintaining a *fixed temperature* (energy intensive) and keeping the operational *temperature below a defined maximum threshold* (less energy intensive). Both were modelled to compare their effects on system performance. For *C. vulgaris*, the annual biomass productivity at a fixed temperature was only slightly higher than when the operational temperature was kept below a maximum threshold; this was the case for both continuous and batch cultivation (as shown in Fig.9 and Table 2).

For *C. pyrenoidosa*, when the operational temperature was kept below a fixed maximum, the predicted biomass productivity was substantially reduced than when it was maintained at a fixed level (Fig.9 and Table 2). A temperature of 38.7℃ was found to be close to optimum for *C. pyrenoidosa* regardless of the light intensity, according to the *P-I* curve derived from Bernard [19]. As a result, lower biomass productivities were obtained at temperatures held below 38.7 ℃.

C. vulgaris exhibited greater flexibility under an optimum temperature depending on light intensity (Appendix C, Fig.C.1). Thus, no significant difference in biomass productivities was observed under these two different temperature regimes.

The distance between reactors also affects the reactor temperature (Fig.11) as incident light and temperature are linked. The average and maximum PBR temperature therefore rise with increasing PBR spacing until they approach the temperature of a single isolated PBR. Compared to the small diameter reactors, the PBRs with large diameters have low temperatures under sub-tropical climate conditions in Brisbane, due to their small surface area to volume ratio and higher thermal mass. The maximum temperatures in large diameter reactors are also more stable when the distances between reactors increase. This is due to the higher specific heat capacity of the larger volume in the latter. Consequently, reducing the distance between PBRs and/or increasing reactor diameter could be an effective alternative to reduce heat load and culture temperature fluctuations, especially for microalgae strains with a narrow optimal temperature range, if this reduction in reactor spacing and/or increase in PBR diameter does not result in a significant decline in microalgae growth rate.

Although it is necessary to control constant optimal temperature to achieve maximum biomass productivity, it is economically unfeasible to run commercial outdoor systems at a constant temperature except for very high value products because of the huge

amount of heat energy that must be balanced, through supply and/or dissipation (Table 2). Microalgae cultivation in outdoor PBRs generally therefore has to be controlled to stay below the maximum temperature threshold. This can be achieved using a heat exchanger or by spraying cooling water onto the PBR surface [31].

In all, the model developed integrates principle formulas that has been widely used and well recognized, together with several assumptions (e.g. well mixed in PBR, constant biomass loss rate due to respiration during night over year, constant biomass concentration during daytime over year). These assumptions have been reported in other work [5, 6], and our estimates are in a comparable range to similar studies. The next phase of this study will involve cultivation experiments to validate this theoretical model.

4. Conclusion

A comprehensive biomass productivity model has been presented for arrayed cylindrical PBRs. It enables the analysis of the effects of solar shading, the 'canyon effect' of diffuse and reflected light, and the influence of temperature on algae growth as a function of PBR height, spacing, orientation and culture density. The model shows that the volumetric biomass productivity of arrayed PBRs can be significantly lower than that of a single PBR due to shading effects on light, despite some benefits on cooling, and that optimisation is therefore essential for effective commercial operation. Moreover, the algae species in this study had a high temperature threshold, suitable for the location. Species preferring lower temperature would benefit from tighter spacing distances between PBRs due to cooling effects. The predicted maximum areal biomass productivity occurred at a reactor spacing distance to height ratio that provided a balance between high volumetric biomass productivity per reactor (g L^{-1} d^{-1}) and total

areal reactor volume (L ha^{-1}, as a function of number of reactors per footprint). Specifically, this can be optimised by adjusting the spacing distance between PBRs relative to the reactor height and the biomass concentration for a given system configuration. The biomass productivity improvement through increased PBR height was limited as more solar shading occurs. For *C.vulgaris*, in the variable range analysed, the optimal system configuration was achieved with a PBR diameter of 0.15 m, height 1 m, and spacing distance 0.1 m using 0.3 g L^{-1} biomass concentration for continuous culture and this delivered a biomass productivity of 55.65 t ha^{-1} yr^{-1}. A spacing distance of 0.1 m, however, is impractical for operation. If using a reasonable spacing, such as 0.4 m, and remaining the other best configuration (PBR diameter of 0.15 m, height 1 m, and spacing distance 0.1 m using 0.3 g L^{-1} biomass concentration), a biomass productivity of 28.3 t ha^{-1} yr^{-1} was achieved. While lower, it is anticipated that the capital costs would also reduce per unit area. To determine the overall effect of these design differences this model can be coupled to techno-economic models to define the optimal product design on a production cost per kilo basis.

Algae species exhibited large differences in biomass productivity due to their different photosynthetic/respiratory characteristics which control growth yield. This, in turn, resulted in different optimal PBR array layouts for each species analysed. The model developed provides a useful tool to guide the design of microalgae production systems toward optimal biomass productivity by considering more comprehensive aspects, not only for biomass production but also the temperature control, which could facilitate the development of best design on large-scale photobioreactor system and economical algae cultivation process.

Acknowledgements

This study is supported by the CSC scholarship, 'Yuanzhi' project of School of Biotechnology of East China University of Science and Technology and the Science and Industry Endowment Fund (John Stocker Postdoctoral Fellowship PF16-087).

Declarations of interest: none.

No conflicts, informed consent, human or animal rights applicable.

Authors' contributions All authors performed conception and design of the study. JH, and JY performed technical and logistic support. JH performed data analysis and interpretation. JH drafted the manuscript. JH, JY and BH wrote manuscript. JY and BH performed critical revision of the manuscript. BH obtained funding and designed the overall project. All authors read and approved the final manuscript. All authors (J. Huang; jkehuang@163.com; J. Yarnold; j.yarnold@uq.edu.au and B. Hankamer; b.hankamer@imb.uq.edu.au) take responsibility for the integrity of the work as a whole.

Reference

[1] G.P.'t Lam, M.H.Vermuë, M.H.M.Eppink, R.H.Wijffels, C.van den Berg, Multi-product microalgae biorefineries: from concept towards reality, Trends Biotechnol. 36 (2018) 216-227

[2] Q.Huang, F.Jiang, L.Wang, C.Yang, Design of photobioreactors for mass cultivation of photosynthetic organisms, Engineering 3(2017)318-329

[3] J.Wolf, E. Stephens, S. Steinbusch, J. Yarnold, I.L. Ross, C. Steinweg, A. Doebbe, C. Krolovitsch,S. Müller, G. Jakob, O. Kruse, C. Posten, B. Hankamer, Multifactorial comparison of photobioreactor geometries in parallel microalgae cultivations, Algal. Res.15 (2016) 187-201

[4] E.Stephens, I.Ross, J.H. Mussgnug, L.D. Wagner, M.A.Borowitzka, C. Posten, O. Kruse,B.Hankamer, Future prospects of microalgal biofuel production systems, Trends Plant Sci. 15 (2010)554-564

[5] P.M. Slegers, R.H.Wijffels, G.van Straten, A.J.B.van Boxtel, Design scenarios for flat panel photobioreactors, Appl. Energy 88(2011) 3342–53

[6] P.M.Slegers, P.J.M.van Beveren, R.H.Wijffels, G.van Straten, A.J.B.van Boxtel,

Scenario analysis of large scale algae production in tubular photobioreactors. Appl. Energy 105 (2013) 395-406

[7] G. C.Zittelli, L.Rodolfi, N.Biondi, M.R. Tredici, Productivity and photosynthetic efficiency of outdoor cultures of *Tetraselmis suecica* in annular columns, Aquaculture 261(2006) 932–943

[8] L.Gouveia, S. Graça, C. Sousa , L. Ambrosano, B. Ribeiro, E. P.Botrel, P.C.Neto, A.F.Ferreira, C.M.Silva, Microalgae biomass production using wastewater: Treatment and costs Scale-up considerations, Algal Res. 16 (2016)167–176

[9] M. H. Wilson, D. T. Mohler, J. G. Groppo, T. Grubbs, S.Kesner, E. M. Frazar, A.Shea, C.Crofcheck, M.Crocker, Capture and recycle of industrial CO_2 emissions using microalgae, Appl. Petrochem Res.6 (2016) 279–293

[10] M. K. Lam, K. T. Lee. Cultivation of *Chlorella vulgaris* in a pilot-scale sequential-baffled column photobioreactor for biomass and biodiesel production. Energy Convers. Manag. 88 (2014) 399-410.

[11] L.Xu, P.J.Weathers, XR. Xiong, CZ. Liu, Microalgal bioreactors: Challenges and opportunities, Engineering in Life Science 9 (2009) 178-189

[12] Q. Béchet, A. Shilton, B. Guieysse. Full-scale validation of a model of algal productivity, Environ. Sci. Technol. 48(2014)13826−13833.

[13] K. Loubiere, E. Olivo, G.Bougaran, J.Pruvost, R. Robert, J.Legrand.A new photobioreactor for continuous microalgal production in hatcheries based on external‐loop airlift and swirling flow, Biotechnol. Bioeng. 102(2009)132-147

[14] Q. Béchet, R. Munoz, A. Shilton, B.Guieysse. Outdoor cultivation of temperature-tolerant *Chlorella sorokiniana* in a column photobioreactor under low power-input, Biotechnol. Bioeng. 110 (2013) 118-126.

[15] R.Bosma, E.Zessen, J. H. Reith, J.Tramper, R.H.Wijffels, Prediction of volumetric productivity of an outdoor photobioreactor, Biotechnol. Bioeng.97 (2007) 1108-1120

[16] A. S. Mirón, M.C.C.Garcí, F.G.Camacho, E.M.Grim, Y. Chisti, Growth and biochemical characterization of microalgal biomass produced in bubble column and airlift photobioreactors: studies in fed-batch culture, Enzyme Microb.Technol. 31(2002) 1015-1023

[17] G.C.Zittelli, L.Rodolfi, M. R. Tredici, Mass cultivation of *Nannochloropsis* sp. in annular reactors, J. Appl. Phycol. 15(2003) 107–114

[18] CY. Chen, KL. Yeh, R.Aisyah, DJ. Lee, JS.Chang, Cultivation, photobioreactor design and harvesting of microalgae for biodiesel production: A critical review, Bioresour. Technol. 102(2011) 71–81

[19] O. Bernard, B. Rémond, Validation of a simple model accounting for light and temperature effect on microalgal growth. Bioresour Technol. 123(2012) 520–527

[20] A.Kumar, S. Ergas, X. Yuan, A. Sahu, Q.Zhang, J. Dewulf, F. X.Malcata, H. Langenhove, Enhanced CO_2 fixation and biofuel production via microalgae: recent developments and future directions, Trends Biotechnol.28 (2010) 371-380

[21] J. A. Duffie, W. A. Beckman, Solar engineering of thermal processes 2013; p1-41.

[22] E.M.Grima, F.G.A. Ferna´ndez, F.G.Camacho, Y. Chisti. Photobioreactors: light regime, mass transfer, and scale up, J. Biotechnol. 70 (1999) 231–247

[23] Q. Bechet, A.Shilton, O. B. Fringer, R. Munoz, B. Guieysse, Mechanistic modeling of liquid temperature in outdoor photobioreactors, Environ. Sci. Technol. 44(2010) 2197-2203

[24] Q. Béchet, P.Chambonnie`re, A. Shilton, G.Guizard, B.Guieysse, Algal productivity modeling: a step toward accurate assessments of full-scale algal cultivation, Biotechnol. Bioeng. 112(2015) 987-996.

[25] C. Sorokin, R.W Krauss, Effects of temperature and illuminance on *Chlorella* growth uncoupled from cell division, Plant Physiol. 37(1962) 37–42.

[26] Q. Béchet, A. Shilton, B. Guieysse, Modeling the effects of light and temperature on algae growth: state of the art and critical assessment for productivity prediction during outdoor cultivation, Biotechnol. Adv. 31(2013) 1648-1663

[27] Han F, Wang W, Li Y, Shen G, Wan M, Wang J, Changes of biomass, lipid content and fatty acids composition under a light–dark cyclic culture of *Chlorella pyrenoidosa* in response to different temperature, Bioresour. Technol. 132(2013) 182-189

[28] M.R.Tredici, N.Bassi, M.Prussi, N.Biondi, L.Rodolfi, G.C. Zittelli, G.Sampietro, Energy balance of algal biomass production in a 1-ha “Green Wall Panel” plant: How to produce algal biomass in a closed reactor achieving a high net energy ratio, Appl. Energy 154(2015) 1103-1111

[29] O.Pulz, Photobioreactors: production systems for phototrophic microorganisms, Appl. Microbiol. Biotechnol. 57 (2001) 287-293

[30] J.Ruiz, G.Olivieri, J.d. Vree, R.Bosma, P.Willems, J.H.Reith, M.H.M. Eppink, D.M.M. Kleinegirs, R.Wijffels, M.J.Barbosa, Towards industrial products from

microalgae, Energy Environ. Sci. 9(2016)3036-3043

[31] A.P. Carvalho, L.A. Meireles, F.X. Malcata, Microalgal Reactors: a review of enclosed system designs and performances. Biotechnol. Prog. 22(2006)1490-506

[32] M.Collares-Pereira, A. Rabl, The average distribution of solar radiation-correlations between diffuse and hemispherical and between daily and hourly insolation values, Sol. Energy 22(1979)155-164

[33] F. G. Acien Fernandez, F. Garcıa Camacho, J. A. Sanchez Perez, J. M. Fernandez Sevilla, E. Molina Grima. A model for light distribution and average solar irradiance inside outdoor tubular photobioreactors for the microalgal mass culture, Biotechnol. Bioeng. 55(1997) 701-714

[34] F.G. Camacho, A.C. Gómez, F.G.A.Fernández, J.F. Sevilla, E.M. Grima, Use of concentric-tube airlift photobioreactors for microalgal outdoor mass cultures. Enzyme Microb. Technol. 24(1999) 164-172

[35] D. Robinson, A. Stone, Solar radiation modelling in the urban context, Sol. Energy 77(2004) 295-309

[36] J. Yarnold, Photosynthesis of microalgae in outdoor mass cultures and modelling its effects on biomass productivity for fuels, feeds and chemicals. Thesis submitted for the degree of Doctor of Philosophy, The University of Queensland, Brisbane Australia (2016).

[37] J. Roles, J. Yarnold, K. Hussey, B. Hankamer. Business models and policy settings for a global microalgae-based sustainable fuel industry. In review, Nature Sustainability, October 2018.

Appendix A. Light model

A.1 Hourly radiation calculated from daily radiation

According to Collares-Pereira et al. [32], light intensity, I_0 (μmol m^{-2} s^{-1}), can be estimated from daily radiation (H_d, W m^{-2}). The daily radiation data of Brisbane is available from the Bureau of Meteorology of Australia .The following equation represents their correlation.

$$\frac{I_0}{H_d} = (a + b \cdot \cos w) \cdot \frac{\pi \cdot (\cos w - \cos w_s) \cdot E_f}{24 \cdot \left(\sin w_s - \frac{\pi \cdot w_s}{180} \cdot \cos w_s \right)} \quad \text{(A.1)}$$

E_f is the photosynthetic efficiency factor, converting W m^{-2} to μmol m^{-2} s^{-1} (E_f= 1.98) .The coefficients a and b are shown as following.

$$a = 0.409 + 0.5016 \cdot \sin(w_s - 60) \quad \text{(A.2)}$$

$$b = 0.6609 - 0.4767 \cdot \sin(w_s - 60) \quad \text{(A.3)}$$

w is solar hour angle, given as:

$$w = 15 \cdot (h - 12) \quad \text{(A.4)}$$

Where h is the solar time of hour at day, which is related to real time, longitude of reactor location, meridian of the reactor location, and the equation of time [5].

w_s is the sunset hour angle which is expressed as Eq. (A.5).

$$w_s = \cos^{-1}(-\tan\phi \cdot \tan\delta) \quad \text{(A.5)}$$

Where, ϕ is the latitude of location, δ is the solar declination.

$$\delta = 23.45 \cdot \sin\left[\left(\frac{360}{365}\right) \cdot (284 + n)\right] \quad \text{(A.6)}$$

Where n is the day number in the year.

The diffuse light intensity can be calculated by Eq. (A.7) [32]

$$I_{diff\_horizontal} = \begin{cases} 0.99 \cdot I_0 \text{ ---------- } K_t \le 0.17 \\ (1.188 - 2.272 \cdot K_t + 0.9473 \cdot K_t^{\,2} - 21.865 \cdot K_t^{\,3} + 14.648 \cdot K_t^{\,4}) \text{ -- } -0.17 \prec K_t \le 0.75 \\ (-0.54 \cdot K_t + 0.632) \cdot I_0 \text{ ---------- } 0.75 \prec K_t \le 0.8 \\ 0.17 \cdot I_0 \text{ ---------- } K_t \succ 0.8 \end{cases} \quad \text{(A.7)}$$

The direct incident radiation is obtained by Eq. (A.8)

$$I_{dire\_horizontal} = I_0 - I_{diff\_horizontal} \quad \text{(A.8)}$$

The daily clearness index K_t, is defined as the ratio between the daily radiation (H) on the horizontal surface at ground level and the daily extraterrestrial radiation (H_O) [21].

$$K_t = \frac{H_d}{H_O} \quad \text{(A.9)}$$

$$H_O = \frac{24}{\pi} \cdot Isc \cdot \left(1 + 0.033 \cdot \cos\left(\frac{360 \cdot n}{365}\right)\right) \cdot \left(\cos\phi \cdot \cos\delta \cdot \cos w_s + \frac{2\pi \cdot w_s}{360} \cdot \sin\phi \cdot \sin\delta\right) \quad \text{(A.10)}$$

Where, I_{sc} is the universal solar constant (1367 W m^{-2}), n is the day of year, ϕ is the latitude of location, δ is the solar declination, w_s is the sunset hour angle.

A.2 Light input for single cylindrical PBR

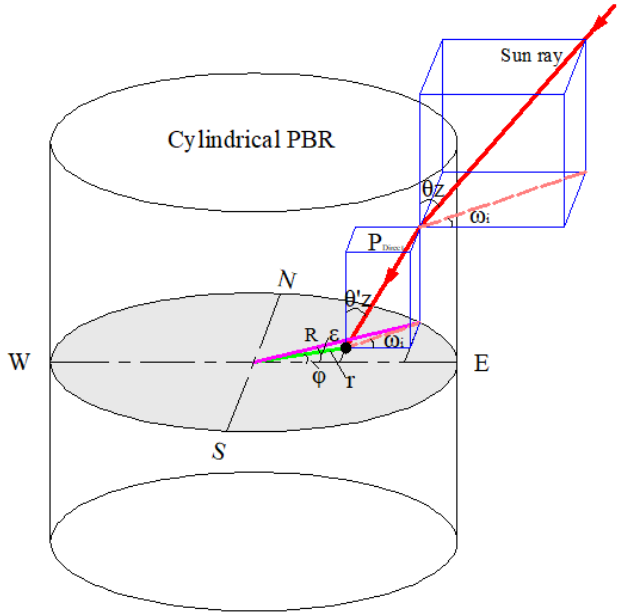

Fig. A.1 Schematic of light transmission inside the cylindrical reactor and various angles associated with light path of direct solar ray(θ_z is zenith angle, ω_i is angular displacement

from east of the projection of beam radiation on the horizontal plane, P_{Direct} is light path of direct light in reactor, *r is p*olar radius of any point inside the reactor in polar coordinate system, *φ is* polar angle of any point inside the reactor in polar coordinate system, R is the reactor diameter, ε is the angle between east direction and line connected circle center and point that sun ray impinges on reactor surface. E is the east direction, N is the north direction, W is the west direction, S is the south direction).

According to Grima et al. [22] and Acien Fernandez et al. [33], the path of direct light in cylindrical reactor is demonstrated in Fig. A.1. For any point inside the reactor (r, ϕ), the light path of direct light can be calculated by Eq. (A.11).

$$P_{Direct} = \frac{R \cdot \cos\varepsilon - r \cdot \cos\varphi}{\cos\omega_i \cdot \sin\theta_z^{'}} \tag{A.11}$$

Where, $\theta^{'}_z$ can be determined using Snell's law as follow [34]:

$$\frac{\sin\theta_z^{'}}{\sin\theta_z} = \frac{n_1}{n_2} \tag{A.12}$$

where n_1 and n_2 are the refractive indexes of air (1.0) and water (1.33), respectively. θ_z is the zenith angle is given as [21]:

$$\theta_z = \cos\left(\sin\phi \cdot \sin\delta + \cos\phi \cdot \cos\delta \cdot \cos\omega\right)^{-1} \tag{A.13}$$

Where, ϕ is the latitude of location, δ is the solar declination and ω is hour angle. ω_i shown in Fig. A.1 is the angular displacement from east of the projection of beam radiation on the horizontal plane, defined as follows:

$$\omega_i = \left|\gamma_S\right| - 90° \tag{A.14}$$

Where, γ_S is solar azimuth angle [21].

$$\gamma_S = sign(\omega) \cdot \left|\cos^{-1}\left(\frac{\cos\theta_z \cdot \sin\phi - \sin\delta}{\sin\theta_z \cdot \cos\phi}\right)\right| \tag{A.15}$$

The sign function is equal to +1 if ω is positive and −1 if ω is negative.

Estimation of ε for any pair (r_i, φ) and ω_i is obtained by iteration in Equation (A.16).

$$\frac{R\cdot\cos\varepsilon - r\cdot\cos\varphi}{R\cdot\sin\varepsilon - r\cdot\sin\varphi} = \tan\omega_i \quad \text{(A.16)}$$

Thus, the local light intensity of direct light at any point (r, φ) can be determined as,

$$I(r,\varphi) = \frac{I_{dire\_horizontal}}{\cos\theta_z}\cdot\exp(-\sigma\cdot C_x\cdot P_{Direct}) \quad \text{(A.17)}$$

where, σ is absorption coefficient ($m^2\ g^{-1}$) and C_x is biomass concentration ($g\ L^{-1}$).

The amount of diffuse light can be calculated by Eq. (A.18) [5].

$$I_{diff\_reactor} = (\frac{1+\cos\beta}{2})\cdot I_{diff\_horizontal} \quad \text{(A.18)}$$

Where, β is the angle that the slope of the reactor surface makes with the surface of the earth.

For the ground reflected diffuse light, it is given as [34]:

$$I_{refl\_reactor} = \rho\cdot(\frac{1-\cos\beta}{2})\cdot\left(I_{dire\_horizontal} + I_{diff\_horizontal}\right) \quad \text{(A.19)}$$

Where, ρ is ground reflectivity.

In addition, according to Slegers [6], the light angle for diffuse and reflected diffuse light is assumed to be perpendicular to the reactor wall.

A.3 Light input for PBRs in full scale arrangement

A.3.1. Direction of light

The zone (yellow (Fig. A.2) is where neighbouring PBRs cause shading to the target PBR column (PBR_t) can be determined according to the azimuth. The range of zone is between the line A and A'. The target column will be shaded by the nearby reactors that are located in this area. As shown in Fig.A.2, the parts of reactor PBR (2, 1), PBR (2, 2) and PBR (3, 3) obviously occupy this zone, which will cause shading to the target reactor (TPBR).

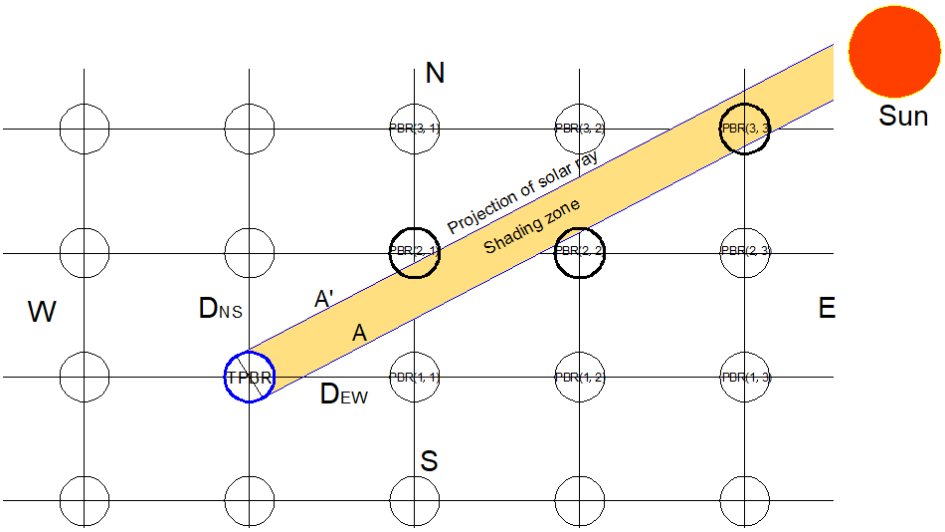

Fig. A.2 Schematic diagram of cylindrical PBRs with configuration parameters and the "shading zone" to the target PBR (PBR_t) depending upon the angle of the sun (E is the east direction, N is the north direction, W is the west direction, S is the south direction, D_{EW} is distance between neighboring reactor in east-west direction (center to center), D_{NS} *is the* distance between neighboring reactor in south-north direction (center to center), TPBR is the target photobioreactor, PBR(x,y) is the photobioreactor around the target reactor).

The circumference range and height of shadow on target reactor caused by other surrounding reactors are determined through several auxiliary lines as shown in Fig. A.3.

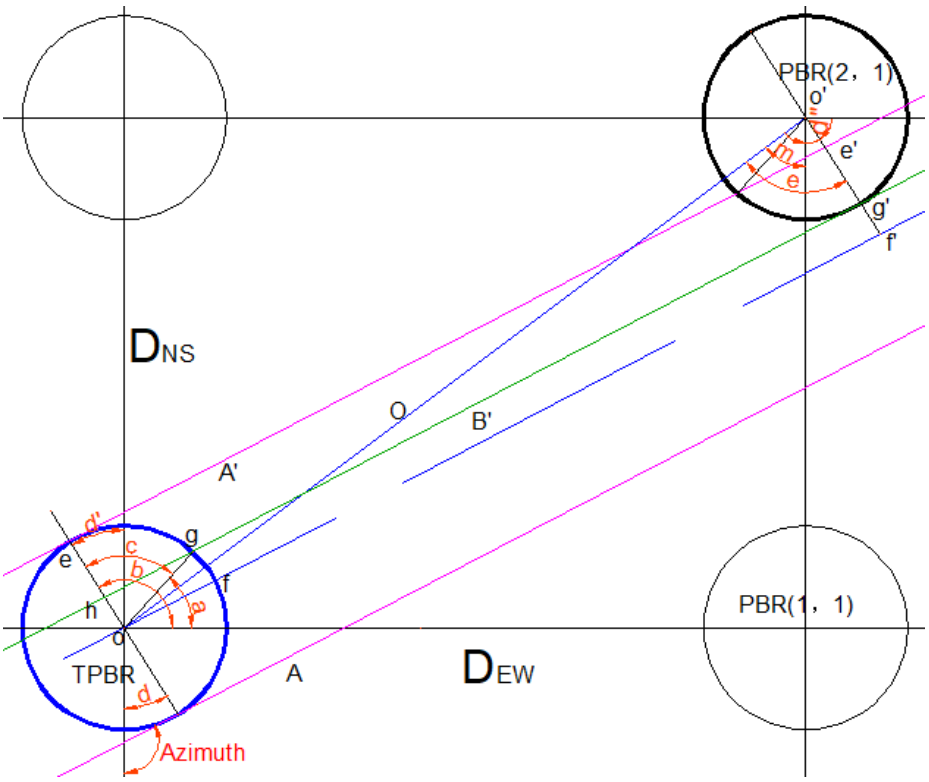

Fig. A.3 The top view of cylindrical reactors with virtual auxiliary lines for calculating shaded circumference of target reactor (E is the east direction, N is the north direction, W is the west direction, S is the south direction, D_{EW} is distance between neighboring reactor in east-west direction (center to center), D_{NS} *is the* distance between neighboring reactor in south-north direction (center to center), TPBR is the target photobioreactor, PBR(x,y) is the photobioreactor around the target reactor).

It can be observed that the shaded circumference of target reactors caused by reactor PBR (2, 1) is arc $\overline{ge}$.

The east direction is assumed as 0°. The first shaded point is **g** with corresponding angle $\angle$**a**. The second shaded point is **e** with corresponding angle $\angle$**b.** Therefore, the range of corresponding angle of shaded arc $\overline{ge}$ is from $\angle$**a** to $\angle$**b**. Thus, the next step is to calculate the angle $\angle$**a** and $\angle$**b**.

According to geometry formulas, the following Eq. (A.20-22) can be derived,

$$\left|Azimuth\right| = \angle d + 90° \tag{A.20}$$

$$\angle b = \angle d' + 90° \tag{A.21}$$

$$\angle d = \angle d' \tag{A.22}$$

According Eq. (A20-22), $\angle$b is equal to | Azimuth |.

In addition, According to geometry principles, the following Eq. (A.23-31) can also be obtained.

$$\angle m = \tan^{-1}\left(\frac{D_{EW}}{D_{NS}}\right) \tag{A.23}$$

$$\angle d'' = \angle d \tag{A.24}$$

$$\angle e = \angle m + \angle d'' \tag{A.25}$$

$$oo' = \sqrt{D_{EW}{}^2 + D_{NS}{}^2} \tag{A.26}$$

$$f'o' = oo' \cdot \cos(\angle e) \tag{A.27}$$

$$f'g' = f'o' - R \tag{A.28}$$

$$oh = f'g' \tag{A.29}$$

$$\angle c = \cos^{-1}\left(\frac{oh}{R}\right) \tag{A.30}$$

$$\angle a = \angle b - \angle c \tag{A.31}$$

Thus, the value of angle $\angle$**a** can be determined by Eq. (A 23-31).

The height of shadow on target reactor caused by reactor PBR (2, 1) can be determined by following Eq. (A.32).

$$H_{shaded} = H - \frac{oo'}{\tan(\theta_z)} \tag{A.32}$$

The mathematic program is made and conducted to search the reactors located in the shading zone. Then, according to Eq. (A20-32), the shaded circumference range and shaded height of target reactors caused by each other reactors are calculated respectively. The shaded circumference and height of PBR_t caused by surrounding PBRs on January 1, 5 pm in Brisbane is demonstrated in Fig (A.4). The calculated

azimuth is 74°, which indicates the sun is at west-south direction relative to target reactor. Three PBRs, PBR (2, 1), PBR (1, 3) and PBR (1, 4) produce the shadows to target column (TA). The shaded areas on target PBR produced by each other PBRs are illustrated in Fig. (A.4B). The overall shaded area on target column is the sum of shaded area caused by each other PBR but subtracting overlapped shaded area.

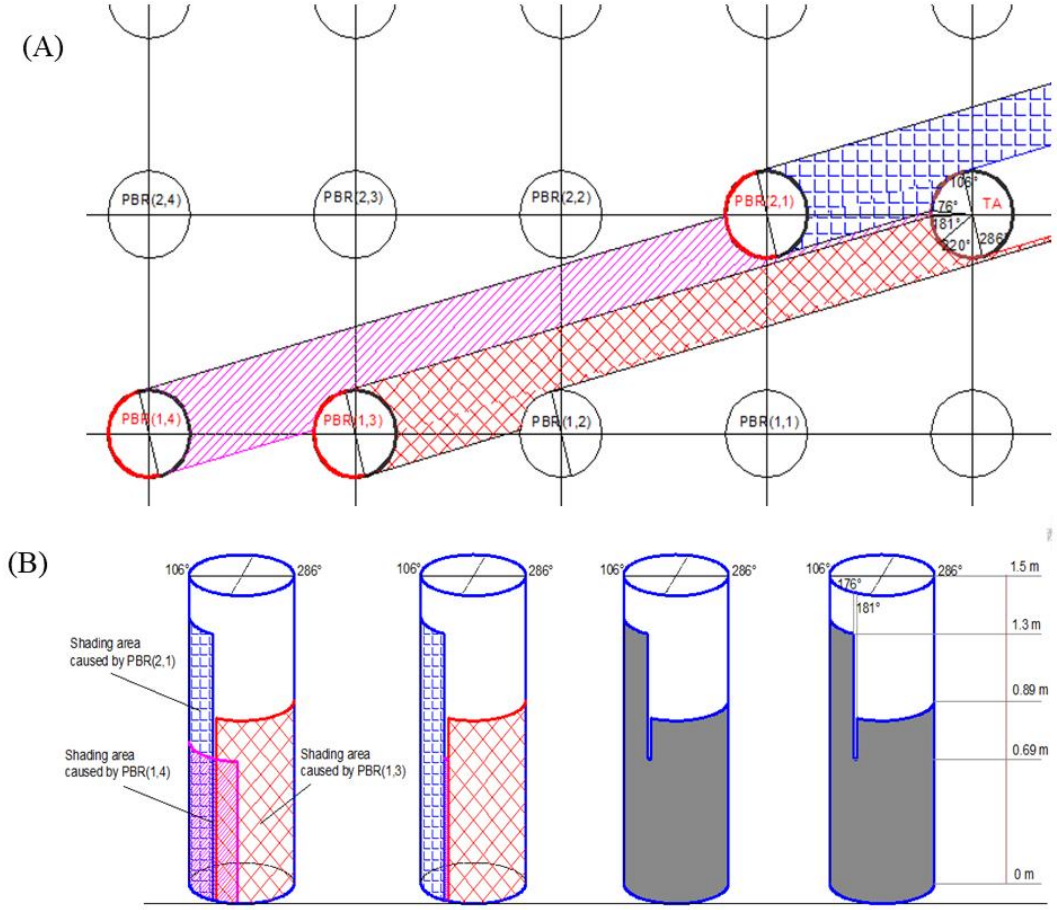

Fig. (A.4) Illustration of the ground shading among cylindrical reactors (A) and shadow on the target reactor (B) (TA is the target photobioreactor, PBR(x, y) is the photobioreactor around the target reactor).

A.3.2. Diffuse light

For multiple PBRs, the canyon effect is considered for diffuse light distribution [6]. The diffuse light on reactor in full scale arrangement is calculated by Eq. (A.33).

$$I_{diff\_reactor} = \left(\frac{1+\cos(\beta+u)}{2}\right) \cdot I_{diff\_horizontal} \quad \text{(A.33)}$$

Where, u is the sky view angle, β is the surface slope. Given the cylindrical reactor geometry feather which is different with flat panel and tubular, Eq (A.34) is derived according to the sky view angle used for flat panel and tubular PBRs [5, 6].

$$u = \tan^{-1}\left(\frac{h'}{L'}\right) \tag{A.34}$$

The sky view angle, u, depends on the height, h', measured from the top of column and the distance between columns. The average distance between the columns, L', is used instead of the distance between two neighboring columns because the columns are discrete distribution. The 'canyon effect' will be significantly overestimated if the distance between neighboring reactors, L_0, is used for calculating the sky view angle. As illustrated in Fig. A.5, L' is calculated by Eq. (A.35) considering the symmetrical distribution of the columns.

$$L' = \frac{a_0}{45}\cdot L_0 + \frac{a_1}{45}\cdot L_1 + \frac{a_2}{45}\cdot L_2 + \frac{a_3}{45}\cdot L_3 + \frac{a_n}{45}\cdot L_n \tag{A.35}$$

In Eq. A.35, n is the number of reactor which intersects with the extension line of the tangent between two nearby reactors (A and B). For example, n = 3 in the situation depicted in Fig. A.5.

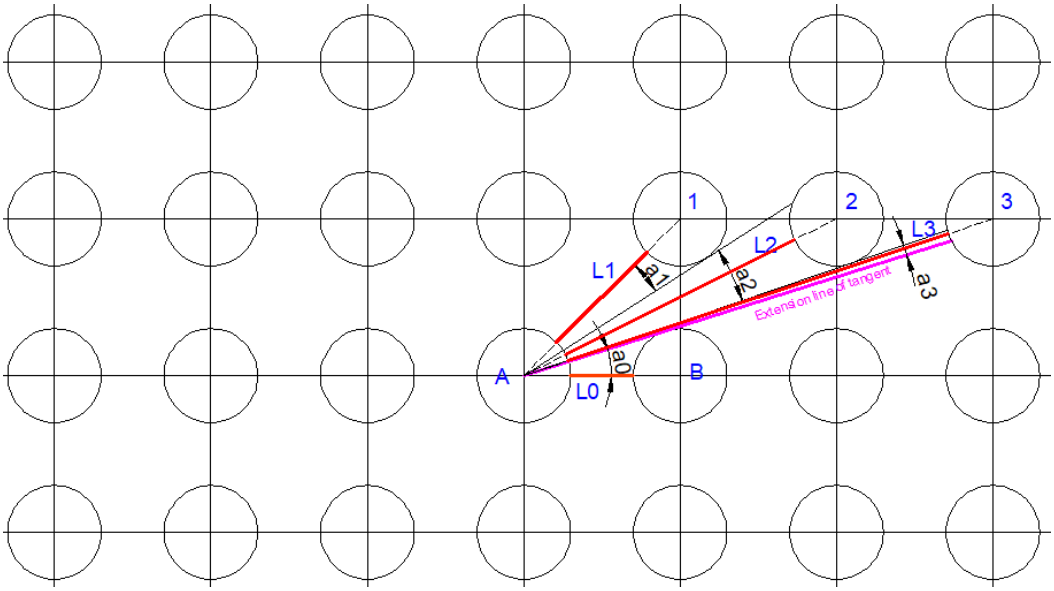

Fig. A.5 Schematic diagram for calculating average distance between reactors (L_n is the

distance between target reactor (A) and other around photobioreactor, a_n is the angle account for around photobioreactor directly projected on target reactor, *n* is the number of reactor which intersects with the extension line of the tangent between two nearby reactors (A and B)).

A.3.3 Ground reflected light

Ground reflected light is calculated based on the studies [6, 35] with some modification to adapt for parallel cylindrical PBRs according to Eq. (A36–42):

$$I_{refl\_reactor} = G_{groundreflected} \cdot \left(I_{diff\_horizontal} \cdot \cos(\eta) + f_{ground\_illu} \cdot I_{dire\_horizontal} \right) \quad \text{(A.36)}$$

$$\eta = \tan^{-1}\left(\frac{2 \cdot \left(H_{PBR} + H_{base} \right)}{L'} \right) \quad \text{(A.37)}$$

$$f_{ground\_illu} = \frac{S_{square} - S_{reactor\_ground\_shading}}{S_{square}} \quad \text{(A.38)}$$

$$S_{reactor\_ground\_shading} = \frac{H_{PBR} + H_{base}}{\tan(90° - \theta_Z)} \cdot D_{reactor\_outer} \quad \text{(A.39)}$$

$$S_{square} = D_{EW} \cdot D_{NS} - \pi \cdot \left(\frac{D_{reactor\_outer}}{2} \right)^2 \quad \text{(A.40)}$$

$$G_{groundreflected} = \rho \cdot \frac{1 - \cos\left(\beta - u'(h) \right)}{2} \quad \text{(A.41)}$$

$$u'(h) = \tan^{-1}\left(\frac{h + \mathrm{H}_{base}}{L'} \right) \quad \text{(A. 42)}$$

Where, $h_{reactor}$ is the reactor height (m), H_{base} is the height of the base (m), $D_{reactor\_outer}$ is the outer diameter of reactor (sum of inner diameter of reactor and thickness of reactor wall, assumed to be3 mm), D_{EW} and D_{NS} is the distance between neighbor reactor in east-west direction and south-north direction respectively (m), ρ is the ground reflectivity (dimensionless, with 0.2 used for concrete). It is assumed that D_{EW} is equivalent to D_{NS} to achieve uniform distribution of cylindrical reactors, however, it is

possible to include discrete distances at either angle in the model to simulate other system configurations by just modifying a part of the light model. The sky view angle for ground reflection *u'* is dependent on the reactor height, *h,* measured from the bottom and the average distance between the columns *L'*.

In addition, the light transmission to reactor from the top of the cylindrical reactor is also considered. The light reflected from the surrounding reactors to the target reactor is assumed to be negligible in comparison with direct light, diffuse light and ground reflected light.

Appendix B. Temperature model

The equation that describes the heat balance in a cylindrical PBR is given as [23]:

$$\rho_w \cdot V_r \cdot Cp_w \cdot \frac{dT_r}{dt} = Q_{ra,r} + Q_{ra,dire} + Q_{ra,diff} + Q_{ra,grefl} + Q_{ra,a} + Q_{ra,arefl} + Q_{ra,g} + Q_c + Q_{ev} + Q_b + Q_{cond} \quad \text{(B.1)}$$

where T_r is the reactor liquid temperature (K); ρ_w and Cp_w are the density (kg m^{-3}) and the specific heat capacity (J kg^{-1} K^{-1}) of culture broth, respectively; V_r is the volume of the liquid (m^3); $Q_{ra,r}$ is the radiation from the reactor itself (W); $Q_{ra,dire}$ is the direct solar radiation (W); $Q_{ra,diff}$ is the diffuse solar radiation (W); $Q_{ra,grefl}$ is solar radiation reflected from the ground (W); $Q_{ra,a}$ is the radiation from the air surrounding the reactor (W); $Q_{ra,arefl}$ is the air radiation reflected from the ground (W); $Q_{ra,g}$ is the radiation from the ground (W); Q_c is the convective flux (W); Q_{ev} is the evaporative heat flow (W); Q_b is heat flow into air bubbles (W); and Q_{cond} is the conductive flow with the ground surface at the base surface of the reactor (W).In this balance, the heat capacity of the reactor wall was considered negligible when compared to the heat capacity of the liquid phase.

The detail of each term on the right of Eq. (B.1) can be found in Bechet's work [23]. In our case the shading effect of direct light, the 'canyon effect' of diffuse and ground

reflected light was considered in calculation of the direct solar radiation, diffuse solar radiation, and solar radiation reflected from the ground to calculate the reactor temperature. The shading effect of direct light on radiation absorbed by reactor was also considered by using a "shading" function set to 0 when the PBR was totally shaded by neighboring PBRs and se to 1 otherwise. Hourly readings of typical annual weather data for Brisbane, including dry bulb air temperature, wind speed, relative humidity and solar radiation used for calculating reactor temperature was obtained from EnergyPlus managed by the National Renewable Energy Laboratory. For simplification, the heat flow from the dilution liquid (medium) and harvested culture broth (left the reactor) for continuous cultivation was not considered here. The temperature model for batch cultivation was assumed to be the same for continuous mode.

Appendix C. Algae growth model

Three different microalgae species, *Chlorella sp 11_H5, Chlorella vulgaris and Chlorella Pyrenoidosa* were used for model simulations.

For continuous mode, the biomass concentration was kept constant during daytime by controlling dilution rate to be equal to the specific growth rate of algae (Eq.C.1). Biomass concentration decreases overnight due to respiration (Eq.C.2). Nightly respiration losses would result in a starting concentration less than that set, meaning that harvest would commence later than the start of the light period resulting in a small overestimate in predicted productivities. The biomass loss rate during night can be calculated by Eq.C.4. The annual average volumetric biomass productivity (P_{vol}) can be calculated from biomass productivity during daytime minus biomass loss rate during night (Eq. C.5). The areal biomass productivity is calculated by Eq. (C.6).

$$\frac{dC_x}{dt} = \left(\bar{\mu} - \mathrm{Di}(t)\right) \cdot C_x = 0 \qquad \text{(C.1)}$$

$$\frac{dC_x}{dt} = -r_{d\_night} \cdot C_x \quad \text{(C.2)}$$

$$P_{vol\_light} = C_x \cdot \int_{daylight\_hours} Di(t)dt = C_x \cdot \int_{daylight\_hours} \overline{\mu} dt \quad \text{(C.3)}$$

$$P_{vol\_\text{night-loss}} = C_x \cdot (1 - \exp(-r_{d\_night} \cdot t_{night})) \quad \text{(C.4)}$$

$$P_{vol} = P_{vol\_light} - P_{vol\_night-loss} \quad \text{(C.5)}$$

$$P_{areal} = \frac{P_{vol} \cdot V_{PBRs}}{S_{PBRs}} \quad \text{(C.6)}$$

Where, P_{vol_light} is the annual volumetric biomass productivity during light period of day (g L^{-1} d^{-1}), P_{vol} is the annual average volumetric biomass productivity (g L^{-1} d^{-1}), $P_{vol\_night\_loss}$ is biomass loss rate during night (g L^{-1} d^{-1}), P_{areal} is the annual biomass production (t ha^{-1} y^{-1}), $\overline{\mu}$ is the average specific growth rate (h^{-1}), *Di* is the dilution rate (h^{-1}), C_x is the biomass concentration (g L^{-1}), r_{d_night} is the specific death rate during night (h^{-1}), t_{night} is the time during night(h), V_{PBRs} is the total volume of reactors (L), S_{PBRs} is the total area occupied by reactors (m^2).

For batch mode, the underlying equation for microalgae growth can be expressed as Eq. (C.7) for daytime and Eq. (C.8) for night, respectively. Average biomass productivity of each batch is obtained by Eq. (C.9) with cultivation period set to 7 days. The annual average volumetric biomass productivity is equal to average biomass productivity of all batches (Eq.10).

$$\frac{dC_x}{dt} = \overline{\mu} \cdot C_x \quad \text{(C.7)}$$

$$\frac{dC_x}{dt} = -r_{d\_night} \cdot C_x \quad \text{(C.8)}$$

$$P(i) = \frac{C_{x\_end}(i) - C_{x\_initial}}{Period\_days} \quad \text{(C.9)}$$

$$P_{vol} = \frac{\sum_{1}^{i} P(i)}{i} \quad \text{(C.10)}$$

Where, $\overline{\mu}$ is the average specific growth rate (h^{-1}), C_x is the biomass concentration (g L^{-1}), r_{d_night} is the specific death rate during night (h^{-1}), P(i) is the biomass productivity of i batch cultivation. i is the number of batch. The total number of batch is 52, rounding number obtained as 365 days divided by cultivation period 7 days. C_{x_end} is the biomass concentration of batch end (g L^{-1}), $C_{x\_initial}$ is the initial biomass concentration (g L^{-1}). The biomass weight loss during the night is inevitable and related to many factors such as night temperature, biomass concentration, and the light condition during daytime [26]. Presently, it seems too complex to quantify accurately the value of weight loss at night. In this case, the specific death rate during night is assumed to be equal to the maintenance coefficient during daytime for *C.* sp *11_H5* and *C. Pyrenoidosa.* For *C. vulgaris,* the specific death rate during night is assumed to be 23.7% higher than maintenance coefficient during daytime [24].

Then, $\overline{\mu}$ is determined at each hour as,

$$\overline{\mu}(t) = \frac{1}{S \cdot H_{PBR}} \int_0^{H_{reactor}} \int_0^{R} \int_0^{2\pi} \mu(t, r, \varphi, z)\, d\varepsilon dr dz \quad \text{(C.5)}$$

Where, *S* is the sectional area of the cylindrical PBR (m^2), H_{PBR} is height of PBR (m), R is the radius of the PBR (m).

For *Chlorella* sp. 11_H5, the Haldane growth model was adopted to calculate the specific growth rate at any point in reactor (Eq. (C.6)). The specific growth rate of *C. sp* 11_H5 under various light intensities at 25 ℃ was determined by culture experiment. The experiment data was fitted with growth model to estimate the model parameters.

$$\mu(t,r,\varphi,z) = \mu_m \cdot \frac{I_{loc}(t,r,\varphi,z)}{K_s + I_{loc}(t,r,\varphi,z) + \frac{I_{loc}(t,r,\varphi,z)^2}{K_i}} - r_d \quad \text{(C.6)}$$

Where, μ_m, K_s, and K_i are model parameters (0.329 h^{-1}, 44 μmol m^2 s^{-1} and 347 μmol m^2 s^{-1} obtained, respectively), r_d is the maintenance coefficient (specific death rate during daytime, 0.014 h^{-1} obtained), I_{loc} is the local light intensity(μmol m^2 s^{-1}).

The specific growth rate of *C. vulgaris* was calculated based on Bechet et al. [24] with the consideration of temperature effect as shown in Eq. (C.7).

$$\mu(t,r,\varphi,z) = \mu_m(T) \frac{\sigma \cdot I_{loc}(t,r,\varphi,z)}{K(T) + \sigma \cdot I_{loc}(t,r,\varphi,z)} - \lambda(T) \quad \text{(C.7)}$$

Where, $\mu_m(T)$, $K(T)$, $\lambda(T)$ are model parameters, which is influenced by temperature. σ is the extinction coefficient (m^2 kg^{-1}). The value of each model parameters at different temperature can be found in [24].

The specific growth of *C. Pyrenoidosa* was calculated by Eq. (C.8-9), including the effect of temperature on growth rate [19].

$$\mu(t,r,\varphi,z) = \mu_{opt}(t,r,\varphi,z) \cdot \phi(T) \quad \text{(C.8)}$$

$$\mu_{opt}(t,r,\varphi,z) = \frac{\mu_{\max} \cdot I_{loc}(t,r,\varphi,z)}{I_{loc}(t,r,\varphi,z) + \frac{\mu_{\max}}{\alpha}\left(\frac{I_{loc}(t,r,\varphi,z)}{I_{opt}} - 1\right)^2} - r_d \quad \text{(C.9)}$$

where α is the initial slope of the light response curve, I_{opt} is the irradiance for which growth is maximal (μmol m^2 s^{-1}), μ_{max} is the maximum growth rate for the optimal irradiance and temperature (h^{-1}), r_d is the maintenance coefficient (0.0083 h^{-1} used)

$\phi(T)$ is the temperature effect term which is determined by the Eq.(C.10).

$$\phi(T) = \frac{(T - T_{\max}) \cdot (T - T_{\min})^2}{(T - T_{\min})\left[(T_{opt} - T_{\min}) \cdot (T - T_{opt}) - (T_{opt} - T_{\max})(T_{opt} + T_{\min} - 2 \cdot T)\right]} \quad \text{(C.10)}$$

Where, parameter T_{min} (°C) is the temperature below which the growth is assumed to

be zero, T_{max} (℃) is the temperature above which there is no growth. T_{opt} (℃) is the optimal temperature. T(℃) is the reactor temperature. The value of these model parameters for *C. pyrenoidosa* can be found in [19]. T_{max}, T_{min} and T_{opt} is 45.8 ℃, 5.2 and 38.7 ℃ for *C. pyrenoidosa*, respectively.

The growth-irradiance response curve of three different algae species with different light intensity is shown in the Fig. C.1. The effect of temperature on growth rate of *C. vulgaris and C. Pyrenoidosa* is also illustrated in Fig. C.1.

The light reflection at the PBR outer wall and light loss due to transmission through reactor wall are also considered before calculating the local light intensity with reference to [5]. Lambert–Beer's law was used to calculate light attenuation in the reactor. The extinction coefficients of *C. sp. 11_H5* and *C. Pyrenoidosa* are 178 $m^2 kg^{-1}$ and 200 m^2 kg^{-1} [26], respectively. For *C. vulgaris*, the extinction coefficient is expressed as $\sigma = A \cdot C_x^{\ B}$ (A=117.4 $m^2 kg^{-1}$, B=-0.2) [24].

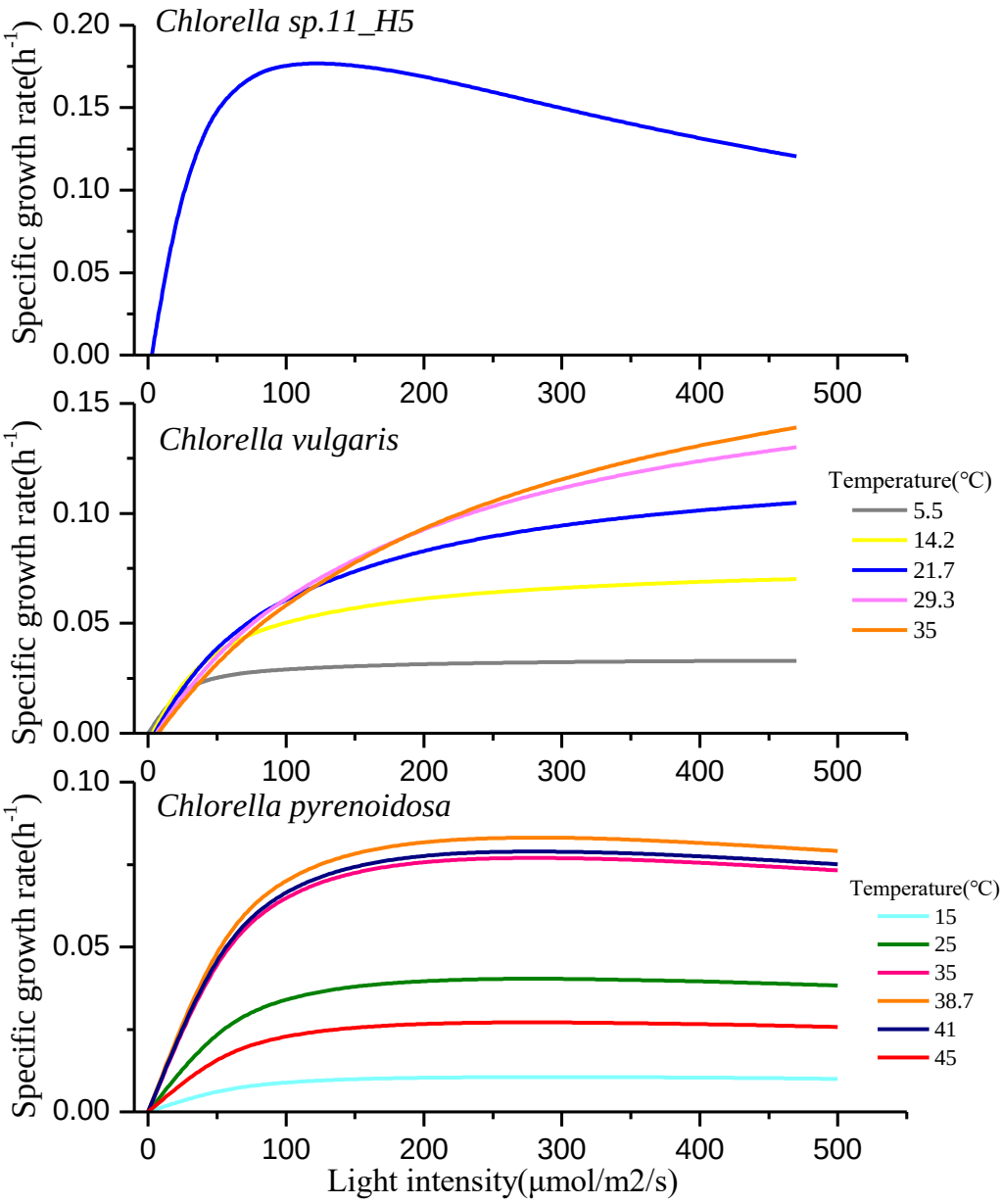

Fig. C.1 Growth-irradiance response curves for *Chlorella* sp.11_H5 [36], *C. vulgaris* [24] and *C. pyrenoidosa* [19].